4-25-2018 10:00 AM

A Mathematical Model for Predicting Rotating Belt Filter Performance

Anthony Sherratt, *The University of Western Ontario*

Supervisor: DeGroot, Christopher T., *The University of Western Ontario*
Co-Supervisor: Straatman, Anthony G., *The University of Western Ontario*
A thesis submitted in partial fulfillment of the requirements for the Master of Engineering Science degree in Mechanical and Materials Engineering

Abstract

Increased demand on wastewater treatment plants has motivated the development of new primary wastewater treatment techniques. Rotating belt filters (RBF) offer a spatially compact and lower cost solution. The goal of the present work is to develop a model that accurately predicts the flow rate capacity and removal efficiency of a generic RBF. Mesh resistance will be characterized using an idealized computational fluid dynamics (CFD) model of the mesh filter used in an RBF. To characterize the cake resistance, a gravity drainage column test was modeled and using the results from the CFD model, the cake resistance versus filtered volume was found. Removal efficiencies were calculated from sieve test data which characterized the effluent concentration of total suspended solids (TSS) for a given filtered volume. The RBF model is extended to include TSS scaling, a PID controller, and parameter optimization to accurately predict steady state and dynamic RBF pilot performance.

Keywords: Filtration, Rotating Belt Filters, Primary Treatment, Computational Fluid Dynamics, Porous Media

Co-Authorship Statement

Chapter 2: Written by Anthony Sherratt, editted by Dr. Christopher DeGroot and Dr. Anthony Straatman.

Chapter 3: Written by Anthony Sherratt, editted by Dr. Christopher DeGroot and Dr. Anthony Straatman

Acknowlegements

I would like to dedicate this thesis to my family, for their unconditional love and support throughout my entire university career. Special thank you to Dr. Chris DeGroot and Dr. Tony Straatman for their guidance and showing me the amazing world of CFD, I greatly look forward to the next 4 years. To Ana for your love and support and Matt for your help manufacturing and running my experiments. Thank you to Dr. Domenico Santoro and the research team at Trojan Technologies for their guidance and the opportunity to work on such a great project. Finally, thank you to my lab mates for making the lab such a great place to work.

Contents

List of Figures

List of Tables

List of Abbreviations, and Nomenclature

Abbreviations

BOD	Biological Oxygen Demand
COD	Chemical Oxygen Demand
CEPT	Chemcially Enhanced Primary Treatment
C-P	Compression Permeability
CFD	Computational Fluid Dynamics
PC	Primary Clarifier
PID	Proportional Integral Derivative
RBF	Rotating Belt Filter
TSS	Total Suspended Solids
WWTP	Wastewater Treatment Plant

Nomenclature

Chapter 1

U	Bulk Fluid Velocity	$[m/s]$
R_{cake}	Cake Resistance	$[1/m^2]$
V	Cumulative Filtrate Volume	$[m^3/m^2]$
μ	Dynamic Viscosity of Fluid	$[Pa \cdot s]$
ρ	Fluid Density	$[kg/m^3]$
L	Length	$[m]$
R_{mesh}	Mesh Resistance (Cake Resistance Model)	$[1/m]$
R_{mesh}	Mesh Resistance (Darcy's law)	$[1/m^2]$
P_o	Operating Pressure	$[Pa]$

ΔP	Pressure Drop	$[Pa]$
s	Solid Mass Fraction	
α_{av}	Stress Averaged Specific Cake Resistance	$[m/kg]$
R_T	Total Resistance	$[1/m^2]$
$\overline{m}$	Wet to Dry Cake Mass Ratio	

Chapter 2

U	Bulk Fluid Velocity	$[m/s]$
K	Darcy Permeability	$[m^2]$
D	Diameter	$[m]$
μ	Dynamic Viscosity of Fluid	$[Pa \cdot s]$
ϵ	Eddy Dissipation Rate	$[m^2/s^3]$
Y_m	Fluctuation Dilation	
ρ	Fluid Density	$[kg/m^3]$
G_b	Generation of Turbulence Kinetic Energy Due to Buoyancy	
g	Gravity	$[m/s^2]$
δ_{ij}	Kronecker Delta	
L	Length	$[m]$
R	Mesh Resistance	$[1/m^2]$
u^*	Normalized Velocity	
ΔP	Pressure Drop	$[Pa]$
a	Resistance Coefficient	
b	Resistance Coefficient	
Re_D	Reynolds Number Based off of Diameter	
$\overline{\rho u_i' u_j'}$	Reynolds Stress	$[N/m^2]$
x	Streamwise Coordinate	$[m]$
t	Time	$[s]$

$\overline{\tau_{ij}}$	Time Averaged Laminar Stress Tensor	$[N/m^2]$
$\overline{P}$	Time Averaged Pressure	$[Pa]$
$\overline{u}$	Time Averaged Velocity	$[m/s]$
C_f	Turbulence Flow Constant	
k	Turbulent Kinetic Energy	$[m^2/s^2]$
σ_ϵ	Turbulence Model Constant	
σ_k	Turbulence Model Constant	
C_μ	Turbulence Model Constant	
$C_{1\epsilon}$	Turbulence Model Constant	
$C_{2\epsilon}$	Turbulence Model Constant	
G_k	Turbulence Production	
u'	Turbulent Velocity Fluctuation	$[m/s]$
μ_t	Turbulent (Eddy) Viscosity	$[m^2/s]$
S_ϵ	User Define Source Term	
S_k	User Define Source Term	
u	Velocity	$[m/s]$

Chapter 3

R_{cake}	Cake Resistance	$[1/m^2]$
V	Cumulative Filtered Volume	$[m^3/m^2]$
$h_{downstream}$	Downstream Water Height	$[m]$
C_{TSSout}	Effluent Concentration of TSS	$[mg/L]$
Δx	Filter Element Length	$[m]$
A	Gravity Drainage Column Test Constant	$[m]$
B	Gravity Drainage Column Test Constant	$[m]$
α	Gravity Drainage Column Test Constant	$[1/s]$
β	Gravity Drainage Column Test Constant	$[1/s]$

Δh	Head Difference	$[m]$
h_{weir}	Height of Weir	$[m]$
h_0	Initial Column Water Height	$[m]$
c	Linear Belt Speed	$[m/s]$
R_{mesh}	Mesh Resistance	$[1/m^2]$
β	Open Area Percentage	
C_0	Sieve Test Model Constant	$[mg/L]$
γ	Sieve Test Model Constant	$[m^2/m^3]$
R_T	Total Resistance	$[1/m^2]$
τ	TSS Scaling Factor	
$h_{upstream}$	Upstream Water Height	$[m]$
Q	Volumetric Flow Rate	$[m^3/m^2 s]$
h_{above}	Water Height Above Weir	$[m]$
h	Water Height in Unit	$[m]$
w	Width	$[m]$

Chapter 1

Introduction and Literature Review

1.1 Background

Wastewater treatment has been a growing concern in recent years. With increased demand placed on wastewater treatment plants (WWTP) in the form of increased levels of pollutants and volume of wastewater needing to be treated [1, 2], it is becoming apparent that newer, more efficient, and less costly solutions are urgently required. Depending on the geographical location, population size, and industrial and agricultural presence, the level and contents in the influent wastewater can differ dramatically [3].

Contaminants in wastewater can be measured by the following: total suspended solids (TSS), biological oxygen demand (BOD), chemical oxygen demand (COD), and turbidity to name a few. Each classification corresponds to a different parameter of importance in the wastewater. The TSS concentration is used to determine the amount of particulate within the wastewater. This is done by pouring a known volume of water over a filter with a nominal pore size ranging from 0.45 to 2.0 [μm] in size. The filter is weighed before and after the experiment, from which, the amount of TSS in the water can be calculated [4, 5]. The BOD test is a method of determining the amount of biological activity in the wastewater and gives an indication of the eventual degradation of organic material. The BOD test takes five days to complete, therefore is limiting in its use for automated systems [6]. The COD test is used

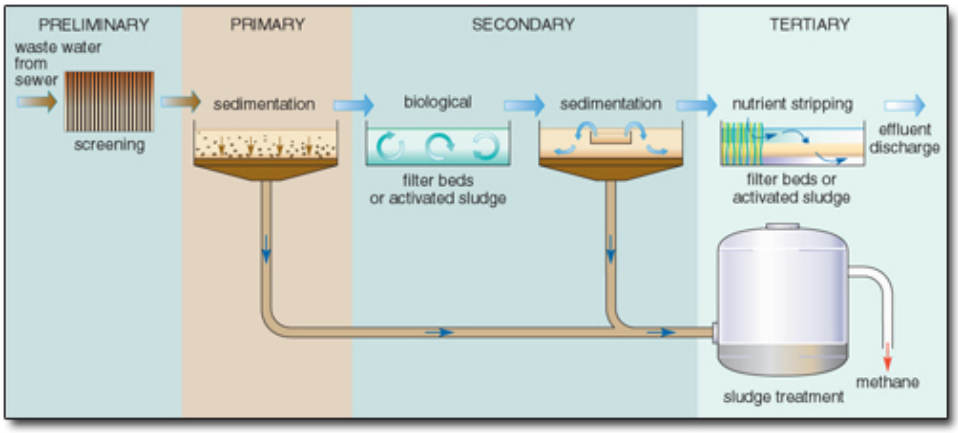

Figure 1.1: Wastewater treatment stages. http://www.open.edu/openlearn/science-maths-technology/science/environmental-science/energy-resources-water-quality/content-section-1.5.1

to measure the oxygen equivalent of the organic material in wastewater that can be oxidized chemically [4]. The benefit to the COD test is it takes significantly less time than the BOD test, however, COD is fractioned into particulate and soluble COD which has no standard definition [4]. Finally, turbidity is a method that characterizes the clarity of the wastewater which can be correlated with TSS.

The four main stages of wastewater treatment, shown in Fig. 1.1, are: preliminary, primary, secondary, and tertiary. Preliminary treatment starts by removing large solids in the influent wastewater by passing it through either screens and/or grit chambers. Primary treatment focuses on the removal of total suspended solids from the influent wastewater, most commonly done through gravity separation. Another form of primary treatment is enhanced primary treatment where a coagulant is added into the influent wastewater stream to increase the size of the particulate allowing for greater removal. Secondary treatment focuses on the removal of organic material through biological and chemical treatment. This process can also include disinfection and nutrient removal. Finally, tertiary treatment is used to remove any remaining suspended solids through micro-filtration or a granular medium. It also is used as a final stage of disinfection and removal of dissolved materials depending on the water reuse application [4].

One of the main concerns regarding wastewater treatment is the removal of particulate in primary treatment. Primary treatment has a considerable effect on further stages of treatment; regarding energy consumption and treatment of organic and inorganic material in the wastewater. The most common method used for primary treatment are primary clarifiers (PC). PCs are a large sedimentation tanks, either circular or rectangular, that vary dramatically in size and capacity depending on the application. Primary influent is pumped into the PC, where during a detention period, the particulates are able to sink to the bottom of the tank by gravity. The sludge is then scraped off the bottom of the tank and transferred to de-watering and further treatment and the clarified surface water is transported to secondary treatment [7]. The issue regarding the use of PCs is their inability to achieve the increasing particulate removal efficiency requirements [8]. The use of chemical enhanced primary treatment (CEPT) is often used, where a chemical coagulant is added to the influent stream, most commonly ferric chloride or polymer for its ability to increase the strength of the resulting amalgamated particulate [9]. This process greatly improves the removal efficiency, however, it increases cost due to the chemicals needed and also increases sludge production.

Rotating belt filters (RBF) are a growing primary wastewater treatment technique. Rather than gravity separation, RBFs remove particulate by utilizing an accumulated layer of particulate (i.e., cake layer) on a mesh filter during the filtration cycle. This cake layer dramatically increases particulate retention as it can filter particles up to three times smaller than the mesh pore size [10]. This cake layer gives the RBF the ability to reach greater than 50% removal efficiency in pilot tests [11, 12, 13, 14] and has also been shown to increase nitrogen removal [15] as well as increase the energy potential of the sludge taken from an RBF unit [16]. RBFs also have been shown to reduce the energy needs in secondary stages of wastewater treatment. By reducing the particle load by 40-60%, the energy consumption in aeration tanks is reduced, there is a greater removal of nutrients, and greater energy recovery in aerobic digestion [17]. They also have a smaller footprint and reduce overhead and operational costs when compared to other primary treatment techniques [18].

With increased demand being placed on WWTPs in the form of increased pollutant levels and stringent effluent wastewater quality, new methods of wastewater treatment techniques are needed. Looking specifically at primary treatment, RBFs offer higher particulate removal efficiencies when compared to PCs, a reduction in overhead costs, and are more spatially compact. It is therefore crucial to develop a model that can quickly and accurately characterize the flow rate capacity and removal efficiencies for various RBFs, under various operating conditions. An RBF model would also be able to be extended to characterize dynamic performance to both to optimize operating parameters and determine the number of units required to meet various WWTPs needs. The topic of modelling techniques that characterize the mesh filters resistance to flow, the growth of the cake layer and its effect on flow during the filtration cycle, and previously proposed RBF models will be discussed in the next section, as a literature review is done on the proposed topic.

1.2 Literature Review

1.2.1 Filtration

Filtration is very common in many engineering fields such as air purification [19], pharmaceuticals [20], and the food and dairy industry [21]. In filtration processes, the goal is to remove suspended particles from the working fluid. This is done by flowing the fluid/particle mixture over a medium where separation occurs due to particle retention on the medium's surface [22]. Despite its popularity in other engineering applications, filtration in primary wastewater treatment is a relatively new concept.

RBFs remove particulate through a combination of sieving and cake filtration. A continually moving, inclined belt filter is used to initially capture particulate in the influent wastewater (i.e., sieving). As the wastewater is gravity fed through the filter the accumulation of particulate on the filter forms a cake layer which transitions the filtration process from sieving to cake filtration. At the end of each rotation of the filter, the cake is cleaned off of the belt by a

physical scraper, air, or water jet. The cake layer that was removed from the belt (i.e., sludge) is then transferred to de-watering, and further treatment and the effluent wastewater is transferred to secondary treatment.

When modelling an RBF, it is crucial to understand and characterize the mesh and cake resistance during the filtration cycle, as it effects both the flow rate capacity of the unit and the removal efficiency.

Depending on the relative size of the influent particles compared to the pore size of the filtration medium, along with the type of medium being used, filtration can be classified into two types: (i) cake and (ii) deep bed filtration [22, 23]. When the pore size of the medium is sufficiently smaller than the diameter of the influent particulate, the particles start to build on the surface of the medium, forming a cake layer. For sufficiently small particles, relative to the pore size, they may penetrate the surface of the medium and deposit within, creating deep bed filtration. A schematic diagram of both filtration mechanisms can be seen in Fig. 1.2.

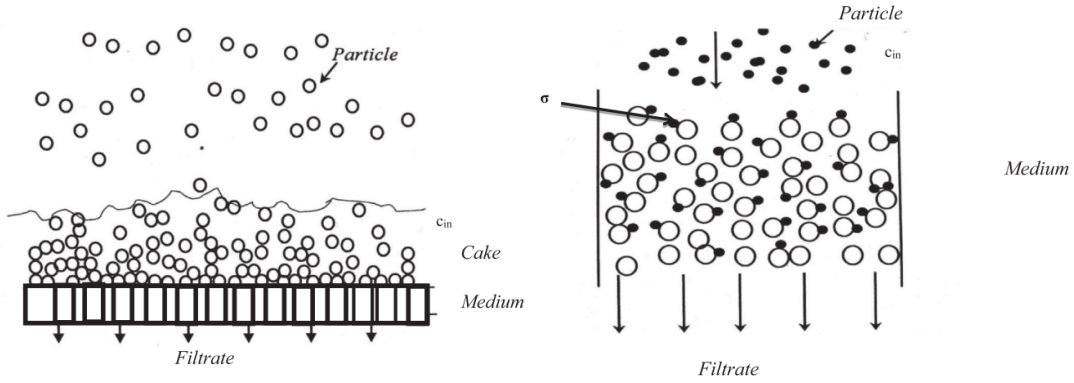

Figure 1.2: Schematic diagrams of (a) cake and (b) deep bed filtration.

Both filtration mechanisms can be pressure or gravity fed through the medium. As the particulate builds on the surface or throughout the filtration medium, an increase in particulate retention can be observed [24]. This accumulation of particulate leads to a decrease in the flow rate of filtered water through the filter [25]. Once the filtration capacity, or the amount of volume that can be filtered before pore plugging [26], is reached, the filtration medium needs

to be either be cleaned or replaced.

1.2.2 Modelling

The flow through a porous medium can be characterized using Darcy's law, which describes the relationship between the pressure drop across the porous media to the velocity of the fluid and the resistance of the media in question. The general form of Darcy's law is shown as

$$\frac{\Delta P}{L} = \mu U R_T \tag{1.1}$$

where ΔP is the pressure drop, L is the length of the porous media, μ is the dynamic fluid viscosity, U is the fluid velocity perpendicular to the porous media, and R_T is the total resistance term. In general for cake filtration on mesh, the resistance to flow is from both the mesh and cake layer, therefore, the total resistance term can be written as

$$R_T = R_{mesh} + R_{cake} \tag{1.2}$$

where R_{mesh} is the mesh resistance and R_{cake} is the cake resistance. Both resistances must be characterized independently of one another, given that the mesh resistance varies with the velocity of fluid and the cake resistance is dependent on numerous other parameters regarding the quality of the influent wastewater. The techniques of modelling each resistance term will be discussed in depth in the following sections.

1.2.3 Mesh Filter modelling

Filters come in many shapes, sizes and materials depending on their application. Materials can vary from metals for electrical safety gear [27], catalytic converters in automobiles [28] and screens for greenhouses [29]; gauze for surgical fabric [30]; plastic and ceramic for wastewater treatment [22, 31]; and sepiolite for ultra-filtration [32]. In each application, it is critical to understand the resistance to fluid flow and it's effect on the process.

The resistance to flow caused by a filter is due solely to the velocity of the fluid passing through it, therefore, it is important to understand how the resistance changes with increased velocity. For low Reynolds number flows (Re < 1), Darcy's law, Eq. 1.1, shows that the pressure drop across a porous medium is linearly proportional to the bulk fluid velocity. However, with an increased Reynolds number, the pressure drop becomes quadratic with respect to velocity and the flow is considered to be in the Forchheimer flow regime [33, 34, 35]. It is therefore important to understand the application the filter will be used in to know how to correctly apply the results obtained when characterizing the filter.

The most common method for characterizing mesh filters is through the use of experiments [27, 28, 36, 37, 38]. Wu et al. [38] described a common approach used to accurately characterize mesh filters. First, the filters need to be classified by weave pattern, with the most common being plain and twill weaves. In a plain weave, the warp (horizontal) wire passes alternatively over and under each weft (vertical) wire and each weft wire passes alternatively over and under each warp wire. In a twill weave, each warp wire passes alternatively over and under two weft wires and each weft wire passes alternatively over and under two warp wires. An example of a both plain and twill weave can be seen in Fig. 1.3. Once classified, the warp and weft wire diameters and the average spacing is measured and averaged at various locations along the filter insert. The filter is then placed in the experimental apparatus. Most commonly compressed air or water are used as the working fluids in mesh characterization experiments. Depending on the working fluid, the flow rate is controlled either by using a valve (for compressed air) or pump (for water). After the valve or pump, the working fluid is then directed through a straightener to ensure uniform flow. It then travels through the filters where pressure transducers pre-and post-filter record the pressure drop for a given fluid flow rate. The results are then used to define coefficients in empirical correlations to determine the resistance to flow for a given Reynolds number.

Another approach that has be taken is the use of computational fluid dynamics (CFD). For the CFD analysis, the filter is using a number of techniques described in literature. Sun et

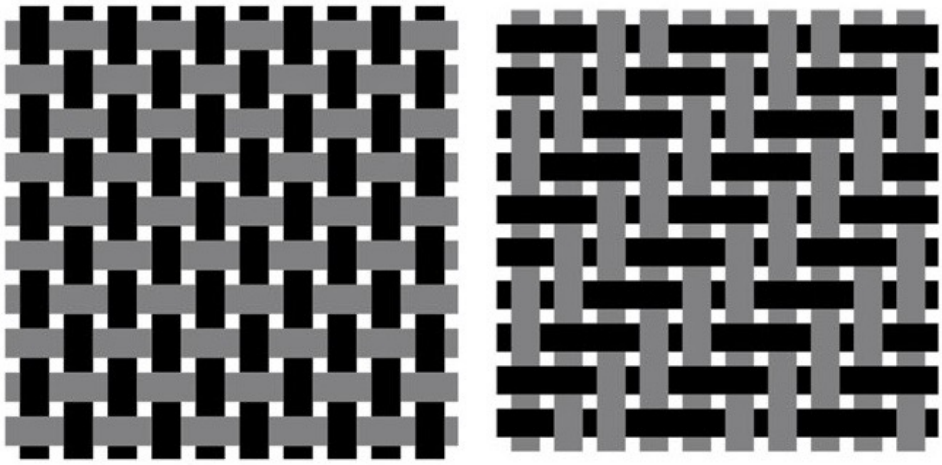

(a) (b)

Figure 1.3: Imagines of (a) plain and (b) twill weave types. http://www.craftyplanner.com/2015/03/02/garment-fabrics-lmsm/

al. [39] modelled filters using three techniques: (i) a complete three dimensional model, (ii) a simplified three dimensional model, and (iii) a simplified two dimensional model. The original three dimensional model was done to best capture the true nature of the mesh being characterized. However, due to the complexity of the mesh being modelled, Sun et al. found that the computational time was immense and therefore attempted a simplified three dimensional which only modelled orthogonal, interwoven wires. The wire geometry was also changed and modelled as a rectangle rather than a cylinder. The effect of reducing the complexity of the model was negligible when comparing the pressure drop across the domain for various fluid velocities, however, the number of grid elements needed to reach grid independence was still large (3.2 million). The simplified two dimensional model was then introduced to further reduce computational time. This was done by eliminating the weave pattern in the filter by removing the vertical wires in the domain. Sun et al. found that this dramatically reduced the computational time and had minimal effect on the resulting pressure drop when compared to the two three dimensional models.

Rather than reduce the geometric accuracy of the model, Teitel [29] hypothesized that filters can be modelled as porous slabs, which will reduce computational time as the porous slab can

reach grid independence with significantly coarser mesh. The coefficients for the source term describing the porous slab were gathered from various empirical correlations corresponding to the filter porosity being modelled. To determine the porous slab technique's accuracy, a three dimensional model was created that captured the true geometry of the various filters being modelled. Like the porous slab, various filter porosities were modelled and it was shown that the three dimensional model closely predicted the pressure drop obtained through empirical correlations gathered from experimental data. However, it was found that the results obtained from the porous slab models were highly dependent on the coefficients used and the type of filter it was replicating.

The techniques for characterizing mesh resistance have their benefits and draw backs. Experiments give the most accurate results given that the variations in the filter geometry and inlet conditions are inherently accounted for. However, the draw backs are the overhead cost to design, manufacture, and build the experimental apparatus which is coupled with the long experimental time needed to characterize each filter. Also, the data obtained through experiments are useful only for the filter being characterized. This means extensive experimental time would be needed if various filters are being characterized. Using CFD offers a reduction in overhead cost and characterization time when compared to experiments, and also allows for generalized models to be created. These generalized models can be used to further characterize other mesh filters used in various applications without the need to run experiments. However, the modelling techniques that are present in the literature have flaws. The two dimensional model that Sun et al. [39] proposed removed the vertical wires. This implies an infinite pore size which greatly increases the complexity of determining the correct thread spacing when applying the model to other mesh types. The porous slab that Teitel [29] proposed did reduce computational time, however, it was found that there was no obvious way to determine which empirical correlation gave the correct pressure drop when compared to the three dimensional and experimental data for a given filter porosity. This, therefore, means an experiment would have to be done on each filter being characterized to guarantee the correct pressure drop. Fi-

nally, no clear boundary conditions were given for either CFD model proposed. Both models modelled the entire filter insert used in the experiment, therefore, the velocity distribution from the experiment should be used as the inlet boundary condition, however, there was no mention of this in either proposed model. These reasons make it very difficult to both model and reproduce the results found. For this reason, it was critical to develop and experimentally validate a CFD model of the mesh filter being used in the final RBF model.

1.2.4 Cake Resistance modelling

Characterizing cake resistance in wastewater filtration can be a complex task. Given the variability in size, shape, and amount of the influent particulate in wastewater, capturing the true resistance to flow caused by the cake build up is quite difficult.

Tien et al. [23, 24, 40, 41] have developed and modified numerous cake resistance models. These models describe both the rate of filtration and the pressure drop across the combination of a mesh and cake layer throughout a filtration cycle. They have also proposed models to quantify the filtration rate and pressure drop depending on the stage of cake filtration; from intermediate blocking of pores during the early stages of cake filtration to fully developed cake filtration where a complete cake layer has formed on the filter mesh. An example of the complete cake filtration model for the rate of filtration and pressure drop are shown in Eqs. 1.3 and 1.4, respectively, obtained from Tien and Bai [40].

$$\frac{dV}{dt} = \frac{P_o}{\mu\left[\frac{\rho s}{1-\overline{m}s}V(\alpha_{av}) + R_m\right]} \tag{1.3}$$

$$P_o t = \frac{\mu\rho s}{2}\left[\frac{\overline{\alpha_{av}}}{1-\overline{m}s}\right]V^2 + \mu R_m V \tag{1.4}$$

where V is the cumulative filtrate volume (per unit width of filter), t is time, P_o is the operating pressure, $\overline{m}$ is the wet to dry cake mass ratio, R_m is the mesh resistance (assumed constant), s is the solid mass fraction, μ is the filtrate viscosity, ρ is the fluid density, and α_{av} is the stress

averaged specific cake resistance. Correlations have also been found to calculate $\overline{m}$, s and α_{av} which are dependent on numerous parameters such as the cake porosity/solidity, particle diameter, and particle density.

The physical parameter describing cake formation is the specific cake resistance, α. As mentioned above, the specific cake resistance or stress averaged specific cake resistance, α_{av}, can be determined from correlations, however, Tien [41] notes that by determining the value of α independently, the true significance of it is better captured in the model. This is done using a compression-permeability (C-P) cell which characterizes the cake layer solidity by compressing a homogeneous solution under a fixed load until mechanical equilibrium is reached. The cake layer height is then measured to determine the overall volume remaining and by knowing the mass of the solids within the cake, the solidity is found. A pressure drop-flow rate experiment can then be done on the cake layer by passing a known velocity of water through the cake layer and measuring the pressure drop. The resulting pressure drop can then be used in Darcy's law to determine the permeability. The combination of the solidity and permeability then gives the specific cake resistance for a given compressive stress.

To include the specific cake resistance data gained from the C-P cell in the cake resistance model, the compressive stress within the cake layer needs to be determined. The compressive stress is caused by the fluid drag acting on the particles within the cake [41]. Knowing this allows for a relationship between the pressure in the pore fluid and the compressive stress to be determined; numerous of which have been proposed and tested. In the work done by Teoh et al. [42] and Bai and Tien [43], the various relationships between the pore fluid pressure and compressive stress were tested for different types of cake layers (created from various materials of differing densities and particle diameters). Both studies found that depending on the type of material used in the filtration experiments and stress relationship used, close agreement between experimental and modelled cake layer growth and total filtration volume was found.

As mentioned previously, there are numerous cake resistance models for varying stages of the filtration cycle, however, to capture the complete cycle, these models would have to be

combined. Ho and Zydney [44] have developed a model that calculates the fluid flux through a fouled membrane over the entire filtration time. Their model takes the flux through a clean filter, then multiplies it by two exponential functions that account for the flow rate through the blocked pores and the reduction of open pores over the filtration cycle. They have found very close agreement between experimental data and the model developed for numerous variations in influent particulate levels.

One of the restrictions on the models mentioned above is that both assume flow normal to the filter. It has been found that the predicted versus actual flux through the cake and mesh layer is significantly less. This is due to a cross flow phenomena where fluid traveling tangential to the cake formation disrupts cake growth by removing particulate from the cake layer. This difference between flux values from mathematical models compared to experiments was first introduced by Green and Belfort [45]. In their findings, they described the difference as a flux paradox. Green and Belfort's goal was a model to predict how much cross flow was needed to reduce premature clogging of filtration processes caused by substantial cake layer growth. This was done by introducing a lift velocity into a lateral migration theory. They found that this addition allowed their model to calculate the right order of magnitude flux whereas previous models would under predict.

With the increased development in cake filtration modelling, Tien and Ramarao [46] have developed another cross flow model to predict the effect of cross flow on cake filtration performance. Their model takes the previous cake filtration model from Eq. 1.3 and introduces a β factor which is the fraction of the particles transported to the medium surface. The β value is dependent on a number of parameters such as the particle diameter, cross flow velocity, and filtration velocity. The proposed model showed close agreement with predicted flux when compared to experimental values.

Despite the accuracy of the cake filtration models, the assumptions that are made when developing the models, the time consuming experiments, along with variables needed, makes them not applicable to RBF modelling. First, the C-P cell test, used to experimentally deter-

mine the cake solidity can take a significant amount of time to reach mechanical equilibrium. Coupled with the uncertainty of choosing the correct relationship between the pore fluid stress and compressive stress for the cake layer being modelled, significant experimental and modelling time is needed. Their models also characterized cake growth over a long filtration period (hours) where the filtration time within an RBF is on the order of seconds. The cake filtration models could be modified to account for the shorter filtration cycle time, however, the experiments needed to validate the model (needed for each different type of influent wastewater) requires significant time given the complexity of experimentally measuring the cake solidity and growth over such a short period of time. Also, the cake and cross flow filtration models are only applicable to either constant pressure or constant flow rate flows. The varying water height along with the inclined filter in an RBF unit means the hydrostatic pressure driving the fluid flow is continuously changing. Coupled with changing influent flow rates, the flux through the RBF unit is also changing continuously. Another assumption these models made was a constant mesh resistance. For low filtration rates, this assumption is applicable, however, for the large flow rates it is known that the mesh resistance is linearly dependent on the fluid velocity. The assumption of a constant mesh resistance has also been addressed by Tien and Ramarao [46], in their cross flow cake resistance model, where they hypothesized that errors in their model could be attributed to the constant mesh resistance assumption. Finally, all of the parameters needed to characterize the cake layer are both time consuming and complex to measure and are continually changing in an RBF.

1.2.5 Current RBF Models

Despite the potential RBFs have as a new primary treatment technique, there are very few experiments or models that have been proposed to characterize their performance. In the following section an experimental and two proposed mathematical models will be discussed.

Rusten and Lundar [47] proposed an experimental apparatus to characterize the hydraulic capacity and removal efficiency of an RBF unit for a given influent TSS concentration. The

experiment, also known as a gravity drainage column test, works by holding a known volume of wastewater, with a known TSS concentration, above a valve. The valve is used to control the flow of water through a filter mesh insert below. The experiment is performed by opening the valve fully, allowing the wastewater to flow through the filter. After the experiment is complete (either when all the water has be filtered or the filter clogs) the effluent water is tested to determine the concentration of TSS from which the removal efficiency is calculated. The hydraulic capacity is then calculated by timing the length of the experiment. This experiment can be performed for various TSS concentration which gives an overall prediction of the hydraulic capacity and removal efficiency.

DeGroot et al. [48] proposed an explicit, two dimensional, dynamic CFD model based on the mass balance of accumulated solids on the belt filter. A general advection equation was used to calculate the accumulation of solids at each element along the filter. The model took experimental pilot data and reverse calculated optimal kinetic coefficients (used to calculate the flow resistance caused by the cake layer) for the model. These kinetics are then used in a forward prediction to observe their agreement between theoretical results and pilot data. The model included a proportional integral derivative (PID) controller which varied the belt speed to maintain a constant unit water height for a varying influent TSS concentration. Close agreement was found between predicted and pilot data for the effluent TSS concentration and linear belt speed prediction for both non-chemically enhanced and chemically enhanced influent wastewater.

Sherratt et al. [49] proposed a one dimensional model to predict the hydraulic capacity and removal efficiency of a RBF unit. Their model starts by mathematically modelling the change in water height over time, of a gravity drainage column test. This model allows for the velocity of the fluid to be calculated and by referencing the water height off of the filter, the pressure drop across the cake and mesh layer can be calculated as the hydrostatic head pressure. The fluid velocity and pressure can be applied to Darcy's law, which allows for a single, effective flow resistance term which combines the mesh and cake resistance together, to be found for a

given amount of filtered volume. This resistance is then applied to the code which calculates the filtered volume and volumetric flow rate per unit area for a given filter belt speed. The total filtered volume through the filter is then used in a mathematical model of a sieve test, where a known volume of wastewater of a known TSS concentration is poured through a mesh sieve thereby removing a portion of the influent TSS. The effluent wastewater is then tested to determine the remaining levels of TSS, giving the removal efficiency for a given amount of filtered volume. Their model shows various predictions for flow rate capacity and removal efficiencies for numerous RBF variations that are predicting values seen in RBF pilots tested throughout the literature.

The models presented show the benefits of modelling RBF units with reasonable predictions of both pilot flow rate capacity and removal efficiencies under steady state conditions and also dynamic performance through the use of a PID controller. However, each models has limitations. The column test experiment gives an overall estimate of the flow rate and removal efficiency, however, do not consider the changing belt speed and water height within an RBF pilot, limiting it's ability to predict RBF pilot installations. The drawback to the two dimensional model, proposed by DeGroot et al. [48], was the large computation time needed to optimize filtration kinetics and then run forward predictions for flow rate capacity and removal efficiency. The one dimensional model, proposed by Sherratt et al. [49], offered considerably lower computational time, however, the one dimensional assumptions limited the accuracy of the predictions. First, the flow through the unit would have to be assumed to be perpendicular to the filter which in an actual RBF is not true given the moving filter causing recirculation zones along the filter. Also, there is no ability to account for the shear along the belt, which effects the formation of the cake layer as it can both inhibit the growth of the cake layer but also transport particulate along the belt, increasing the cake resistance at various locations. Another limitation the one dimensional model has is its calculation of a combined flow resistance. This assumption means that the model cannot be used to model an RBF pilot over the course of a day, for example. The model has to be able to scale its effect resistance with changes in influ-

ent TSS concentration, however, this scaling factor would inherently scale the mesh resistance along with the cake resistance, which is not correct.

1.2.6 Summary

With increased demand on wastewater treatment plants, there is a growing need for a more effective and less costly primary treatment technique. RBFs offer a reduction in overhead and operational costs [18], higher TSS removal efficiencies [11] and reduction in energy needs for secondary treatment [17]. However, despite their potential, there are very few proposed models for characterizing RBF units. The reason for this is likely due to the complex hydrodynamics that are present during the formation of the cake layer during the filtration cycle. Numerous studies have been conducted that attempt to characterize both the mesh resistance and cake resistance, however, these models are limited due to their need for time consuming and costly experimental work to either confirm CFD predictions for the mesh resistance models or determine values to characterize the cake layer in cake resistance models. Along with the experimental need, the cake resistance models presented are not applicable to RBF modelling due to their assumption of either constant pressure or constant flow rate filtration. The RBF models that have been proposed have accurately predicted RBF performance, however, they are limited in their capabilities. The experimental method proposed by Rusten and Lundar [47] gives an overall prediction of capacity and removal efficiency but lacked the belt speed input which effects the cake growth on the filter. DeGroot et al.'s [48] two dimensional model was significantly more advanced, however, the computational time made it impractical. Finally, the one dimensional model proposed by Sherratt et al. [49] reduced computational time significantly, however, the method of combining the mesh and cake resistance did not allow for correct modelling of more than capacity and removal efficiency curves for various RBF units. The goal of this work, which will be discussed in the next section, is to take the existing model from Sherratt et al. [49] and separate the mesh and cake resistance terms. This will allow for accurate TSS scaling and also allow a PID controller to be implemented to dynamically model

RBF performance for varying inlet an operating conditions.

1.3 Objectives of the Present Work

The goal of the present work is to develop a one dimensional RBF model that will accurately predict flow rate capacity and removal efficiency and allow for extensions in the form of a PID controller to characterize dynamic behavior of an RBF unit. The proposed model will be based off of the model developed by Sherratt et al. [49] which will be modified to include separate mesh and cake resistance term.

The specific objectives of this work are as follows:

1. Develop a generalized CFD mesh resistance model that characterizes the pressure drop across various clean mesh filter for varying fluid velocities. The CFD model will be validated using experimental data.

2. Characterize the cake layers resistance to flow during the filtration cycle. This will be done by modelling a gravity drainage column test, whereby using the mesh resistance as a function of fluid velocity obtained from the mesh filter CFD model, the cake resistance can be calculated using Darcy's law.

3. Characterize the removal efficiency by modelling a sieve test which gives the effluent concentration of TSS for given amount of filtered wastewater.

4. Using the above models, develop a one dimensional RBF model that can accurately characterize the flow rate capacity and removal efficiency of a generic RBF for varying operating conditions.

1.4 Thesis Outline

The remaining chapters in this thesis describe the steps taken to achieve the objectives listed above. The chapters will be presented as follows:

- Chapter 2: A generalized three dimensional model of an idealized filter pore will be presented. Boundary condition development will be discussed in detail and theoretical results will be compared to experimental results.

- Chapter 3: A one dimensional RBF model will be presented. Using the mesh resistance gathered from the previous section, a mathematical model for calculating the cake resistance for a given filtered volume will be developed. Both the mesh and cake resistance results will be used to accurately predict RBF pilot capacity and removal efficiency using both a steady state and a quasi-transient PID controlled model.

- Chapter 4: A summary of the present work done and key findings will be given along with recommendations for future work.

Bibliography

[1] Teklehaimanot, G. Z., Kamika, I., Coetzee, M. A., and Momba, M. N., 2015, "Population Growth and Its Impact on the Design Capacity and Performance of the Wastewater Treatment Plants in Sedibeng and Soshanguve, South Africa," Environmental Management, **56**(4), pp. 984–997.

[2] S.L., P. P., G.C., D., and Ehrlich, 2008, "Human Appropriation of Renewable Fresh Water," American Association for the Advancement of Science, **271**(5250), pp. 785–788.

[3] Winkler, I., *Wastewater Treatment : A Road to Safer Society*.

[4] Metcalf and Eddy, 2002, *Wastewater Engineering: Treatment and Reuse*, McGraw - Hill, 4 ed.

[5] ., "Methods of Chemical Analysis of Water and Waste (MCAWW) (EPA/600/4-19/020)," .

[6] Guwy, A. J., Farley, L. A., Cunnah, P., Hawkes, F. R., Hawkes, D. L., Chase, M., and Buckland, H., 1999, "An automated instrument for monitoring oxygen demand in polluted waters," Water Research, **33**(14), pp. 3142–3148.

[7] Wilson, T. E., 2005, *Clarifier Design*, 2.

[8] Rusten, B. and Odegaard, H., 2006, "Evaluation and testing of fine mesh sieve technologies for primary treatment of municipal wastewater," Water Science and Technology, **54**(10), pp. 31–38.

[9] Fabrizi, L., Jefferson, B., Parsons, S. A., Wetherill, A., and Jarvis, P., 2010, "The role of polymer in improving floc strength for filtration," Environmental Science and Technology, **44**(16), pp. 6443–6449.

[10] Tien, C., 2012, *Principles of Filtration*, Elsevier, Oxford, U.K.

[11] Razafimanantsoa, V. A., Ydstebo, L., Bilstad, T., Sahu, A. K., and Rusten, B., 2014, "Effect of selective organic fractions on denitrification rates using Salsnes Filter as primary treatment," Water Science and Technology, **69**(9), pp. 1942–1948.

[12] Rusten, B., Secondary, C. A., Author, C., Rusten, B., Rathnaweera, S. S., Rismyhr, E., Sahu, A. K., Ntiako, J., and Rusten, B., 2017, "Water Science and Technology Rotating belt sieves for primary treatment , chemically enhanced primary treatment and secondary solids separation," , pp. 1–10.

[13] Loop, M., Higby, T., Martini, R., and Rusten, B., 2011, "Particle Size Separation Implications on COD Removal before BNR: A Case Study," Nutrient Recovery and Management, pp. 574–581.

[14] Jansen, R., 2016, "Successful pilot test of rotating belt filters," Filtration + Separation, **53**(4), pp. 26–27.

[15] Rusten, B., Razafimanantsoa, V. A., Andriamiarinjaka, M. A., Otis, C. L., Sahu, A. K., and Bilstad, T., 2016, "Impact of fine mesh sieve primary treatment on nitrogen removal in moving bed biofilm reactors," Water Science and Technology, **73**(2), pp. 337–344.

[16] Paulsrud, B., Rusten, B., and Aas, B., 2014, "Increasing the sludge energy potential of

wastewater treatment plants by introducing fine mesh sieves for primary treatment," Water Science and Technology, **69**(3), pp. 560–565.

[17] Batstone, D. J. and Virdis, B., 2014, "The role of anaerobic digestion in the emerging energy economy," Current Opinion in Biotechnology, **27**, pp. 142–149.

[18] Franchi, A. and Santoro, D., 2015, "Current status of the rotating belt filtration (RBF) technology for municipal wastewater treatment," Water Practice and Technology, **10**(2), pp. 319–327.

[19] Meireles, M., Prat, M., and Estachy, G., 2015, "Analytical modeling of steady-state filtration process in an automatic self-cleaning filter," Chemical Engineering Research and Design, **100**, pp. 15–26.

[20] Christy, C. and Vermant, S., 2002, "The state-of-the-art of filtration in recovery processes for biopharmaceutical production," **147**, pp. 3–6.

[21] Sman, R. G. M. V. D. and Boom, R. M., 2004, "Membrane fractionation of milk : state of the art and challenges," **243**, pp. 263–272.

[22] Tien, C., Ramarao, B. V., and Yasarla, R., 2014, "A blocking model of membrane filtration," Chemical Engineering Science, **111**, pp. 421–431.

[23] Tien, C. and Ramarao, B. V., 2011, "Revisiting the laws of filtration: An assessment of their use in identifying particle retention mechanisms in filtration," Journal of Membrane Science, **383**(1-2), pp. 17–25.

[24] Tien, C., Bai, R., and Ramarao, B. V., 1997, "Analysis of Cake Growth in Cake Filtration : Effect of Fine Particle Retention," **43**(1), pp. 33–44.

[25] Zamani, A. and Maini, B., 2009, "Flow of dispersed particles through porous media âĂŤ Deep bed filtration," Journal of Petroleum Science and Engineering, **69**, pp. 71–88.

[26] Bolton, G. R., Lacasse, D., Lazzara, M. J., and Kuriyel, R., 2005, "The Fiber-Coating Model of Biopharmaceutical Depth Filtration," **51**(11).

[27] Bussière, W., Rochette, D., Clain, S., André, P., and Renard, J. B., 2017, "Pressure drop measurements for woven metal mesh screens used in electrical safety switchgears," International Journal of Heat and Fluid Flow, **65**, pp. 60–72.

[28] Kołodziej, A. and Łojewska, J., 2009, "Experimental and modelling study on flow resistance of wire gauzes," Chemical Engineering and Processing: Process Intensification, **48**(3), pp. 816–822.

[29] Teitel, M., 2010, "Using computational fluid dynamics simulations to determine pressure drops on woven screens," Biosyst. Eng., **105**(2), pp. 172–179.

[30] Chu, C. C. and Rawlinson, J., 1994, "Mathematical modeling of water permeability of surgical fabrics for vascular use," Journal of Biomedical Materials Research, **28**(4), pp. 441–448.

[31] Salehi, E., Madaeni, S. S., Shamsabadi, A. A., and Laki, S., 2014, "Applicability of ceramic membrane filters in pretreatment of coke-contaminated petrochemical wastewater: Economic feasibility study," Ceramics International, **40**(3), pp. 4805–4810.

[32] Wang, Q. K., Matsuura, T., Feng, C. Y., Weir, M. R., Detellier, C., Rutadinka, E., and Van Mao, R. L., 2001, "The sepiolite membrane for ultrafiltration," Journal of Membrane Science, **184**(2), pp. 153–163.

[33] Vafai, K. and Tien, C., 1981, "Boundary and inertia effects on flow and heat transfer in porous media," International Journal of Heat and Mass Transfer, **24**(2), pp. 195–203.

[34] Nield, D. A. and Bejan, A., 2013, "Mechanics of Fluid Flow Through a Porous Medium," Convection in Porous Media, pp. 1–778.

[35] Skjetne, E. and Auriault, J.-L., 2014, "High-Velocity Laminar and Turbulent Flow in Porous Media," CEUR Workshop Proceedings, **1225**(August 1999), pp. 41–42.

[36] Kołodziej, A., Jaroszyński, M., Janus, B., Kleszcz, T., Łojewska, J., and Łojewski, T., 2009, "An Experimental Study of the Pressure Drop in Fluid Flows Through Wire Gauzes," Chemical Engineering Communications, **196**(8), pp. 932–949.

[37] Zhu, Z., Wang, Q., and Wu, Q., 2017, "On the examination of the Darcy permeability of soft fibrous porous media; new correlations," Chemical Engineering Science, **173**, pp. 525–536.

[38] Wu, W. T., Liu, J. F., Li, W. J., and Hsieh, W. H., 2005, "Measurement and correlation of hydraulic resistance of flow through woven metal screens," International Journal of Heat and Mass Transfer, **48**(14), pp. 3008–3017.

[39] Sun, H., Bu, S., and Luan, Y., 2015, "A high-precision method for calculating the pressure drop across wire mesh filters," Chemical Engineering Science, **127**, pp. 143–150.

[40] Tien, C. and Bai, R., 2003, "An assessment of the conventional cake filtration theory," Chemical Engineering Science, **58**(7), pp. 1323–1336.

[41] Tien, C., 2002, "Cake filtration research—a personal view," Powder Technology, **127**(1), pp. 1–8.

[42] Teoh, S.-K., Tan, R. B. H., and Tien, C., 2006, "Analysis of Cake Filtration Data-A Critical Assessment of Conventional Filtration Theory," Wiley InterScience, **52**(10), pp. 3427–3442.

[43] Bai, R. and Tien, C., 2005, "Further work on cake filtration analysis," Chemical Engineering Science, **60**(2), pp. 301–313.

[44] Ho, C. C. and Zydney, A. L., 2000, "A Combined Pore Blockage and Cake Filtration

Model for Protein Fouling during Microfiltration," J Colloid Interface Sci, **232**(2), pp. 389–399.

[45] Green, G. and Belfort, G., 1980, "Fouling of ultrafiltration membranes: lateral migration and the particle trajectory model," Desalination, **35**, pp. 129–147.

[46] Tien, C. and Ramarao, B. V., 2017, "Modeling the performance of cross-flow filtration based on particle adhesion," Chemical Engineering Research and Design, **117**, pp. 336–345.

[47] Rusten, B. and Lundar, A., 2006, "HOW A SIMPLE BENCH-SCALE TEST GREATLY IMPROVED THE PRIMARY TREATMENT PERFORMANCE OF FINE MESH SIEVES," WEFTEC, pp. 1919–1935.

[48] DeGroot, C. T., Sheikholeslamzadeh, E., Santoro, D., Sarathy, S., Lyng, T.-O., Wen, Y., Daynouri-Pancio, F., and Rosso, D., 2016, "Dynamic Modeling of Rotating Belt Filters Enables Design Exploration and Advanced Sizing With Varying Influent Conditions," WEFTEC, **2016**(14), pp. 1158–1168.

[49] Sherratt, A., Degroot, C. T., Santoro, D., Daynouri, F., Mao, S., and Straatman, A. G., 2017, "Development of a Volume-Based Filtration Model for Predicting Full-Scale Rotating Belt Filter Performance in Wastewater Applications," WEFTEC.

Chapter 2

A Numerical Approach for Determining the Resistance of Fine Mesh Filters

2.1 Introduction

Fluid flow through porous meshes, or filters, has many practical applications in science and engineering. Filters can vary dramatically in the material from which they are made, their pore size, and their weave pattern. Generally, the application of the filter will dictate the material needed for the filter. Wire mesh filters are common for electrical safety gear [1], catalytic converters [2], high efficiency heat exchangers [3], and screens for greenhouses [4]; cloth for surgical fabric [5]; plastic, ceramic, or metallic materials for wastewater treatment [6, 7, 8, 9, 10]; and sepiolite (clay) for ultra-filtration [11]. The weave type also varies for different applications. Wu et al. [12] described a number of the most common weave types, with the two most common being: (i) plain weave, where the warp and weft (non-warped) wires passed alternately over and under one another and (ii) twill weave, where each warp wire passes alternatively over two then under two weft wires, and each weft wire passes alternately over two and under two warp wires. Depending on the application, material, and weave type, all filters have the common goal of trapping and removing unwanted particles from the working fluid.

The method for mathematically determining the net effect on flow passing through a porous media is described using Darcy's law. Darcy's law shows that the pressure drop is linearly proportional to the velocity for low Reynolds numbers (Re <1). For higher Reynolds number flows, the pressure drop becomes quadratic in terms of velocity and the flow is considered to be in the Forchheimer flow regime [13, 14, 15]. The most common method for characterizing the flow resistance for different types of mesh filters is to run experiments. Experiments in literature describe the general approach of a pump or compressor driving the working fluid (most commonly air or water) through a horizontal pipe or square tube, allowing the working fluid to flow through the mesh filter being characterized [1, 2, 12, 16, 17]. Pressure transducers are placed before and after the mesh filter to measure the pressure differential, while a flow meter is used to determine the volumetric flow rate through the experimental apparatus. The data is then used to calculate the resistance coefficients. The experimental technique can, however, be costly and time consuming.

Another approach for investigating flow phenomena in porous filters is the use of computational fluid dynamics (CFD), which can be faster and cheaper than experiments. Sun et al. [17] proposed a method for characterizing the pressure across wire filters. They described three models: (i) a three dimensional model that resolved the true geometry of the wire weaves (ii); a simplified three dimensional model with interwoven, orthogonal wires and (iii) a simplified two dimensional model using only horizontally placed wires. Using these three models, Sun et al. [17] found good agreement between experimental data and numerical predictions. They also found that the simplification of the mesh geometry had little effect on the pressure drop across the varying meshes while greatly reducing computational time. However, an issue arises when attempting to apply the two dimensional model to other mesh types. Given that there is inherently an infinite pore size (no vertical threads), there is no clear method for incorporating the thread spacing for a given mesh. This then means an experiment needs to be run for each mesh that needs to be characterized. Also, the boundary conditions were not clear, motivating further study of this aspect.

Teitel [4] proposed a different method of reducing the complexity and computational time for CFD simulations of woven screens. It was hypothesized that by modelling mesh screens as a porous jump, the computational time would be reduced substantially when compared to a 3-D model of the screen, with limited effect on the resulting pressure drop. Two models were compared: (i) a 3-D model of the mesh screen and (ii) a porous jump where the screen permeability and inertial factor were calculated using various empirical correlations. It was found that the porous jump did significantly reduce the computational time, as the porous jump can reach grid independence with a very coarse mesh. However, depending on the method for calculating the permeability and inertial factor, the results, when compared to the 3-D (which matched experimental results very well) and experimental data, ranged from very good to very poor. This range of results depended on the knowledge the modeler had of the screen, for example, knowing the correct thickness ratio between the filter and the porous jump modelled. Therefore, depending on the application and screen type, experiments may still need to be done to determine the correct empirical correlations for the permeability and inertial factors used in the porous jump model.

The present study proposes a generalized method for accurately and efficiently determining the pressure drop across mesh filters using CFD simulations on a representative segment of an idealized filter geometry. First, the flow in the inlet section that leads up to the filter is computed and examined in terms of the normalized velocity and turbulence intensity profiles. This data is then used to develop boundary conditions for the representative filter segment. It will be shown, using experimental data for validation, that the peak velocity should be used as the boundary condition in the filter simulations.

2.2 Theory

The pressure drop across a porous medium is described by Darcy's law, given as

$$\frac{\Delta P}{L} = \frac{\mu U}{K} \tag{2.1}$$

where ΔP is the pressure differential, L is the thickness of the medium, μ is the dynamic viscosity, U is the bulk fluid velocity, and K is the permeability [14, 15, 16]. Equation 1 may also be written in terms of the flow resistance, R, as

$$\frac{\Delta P}{L} = \mu U R \tag{2.2}$$

The permeability, K, and resistance, R, are only constant for low Reynolds numbers based on pore diameter (Re < 1). When observing flows at higher Reynolds numbers, the flow through porous media transitions into the Forchheimer flow regime [4, 13, 14, 15]. Rather than the pressure drop being linearly proportional to the velocity, it also includes a quadratic term and is given as

$$\frac{\Delta P}{L} = \frac{\mu U}{K} + C_f \rho \frac{U^2}{\sqrt{K}} \tag{2.3}$$

where ρ is the fluid density and C_f is a constant that depends on the Reynolds number and pore geometry. The resistance term, R, in Eq. 2.2 can also be modified to show that the resistance is linearly dependent on velocity, by writing as

$$R = a + bU \tag{2.4}$$

where a and b are resistance coefficients.

2.3 Experimental Methods

A schematic diagram of the experimental setup is given in Fig. 2.1. A centrifugal pump delivers water to the inlet pipe through a soft PVC tube connected at the inlet. The water then flows through the rigid PVC inlet pipe of 2.5 [m] length towards the filter adapter, where two square

pieces of PVC are bolted together to form a sealed flange. This was used to secure the various mesh filters tested. The filter adapter was connected to the outlet pipe, again rigid PVC, with the same diameter as the inlet pipe. The outlet was attached to another portion of soft PVC tube that directed the water into an 80 [L] reservoir. The flow rate was measured by timing water flowing into a fixed volume, then weighing the water afterwards.

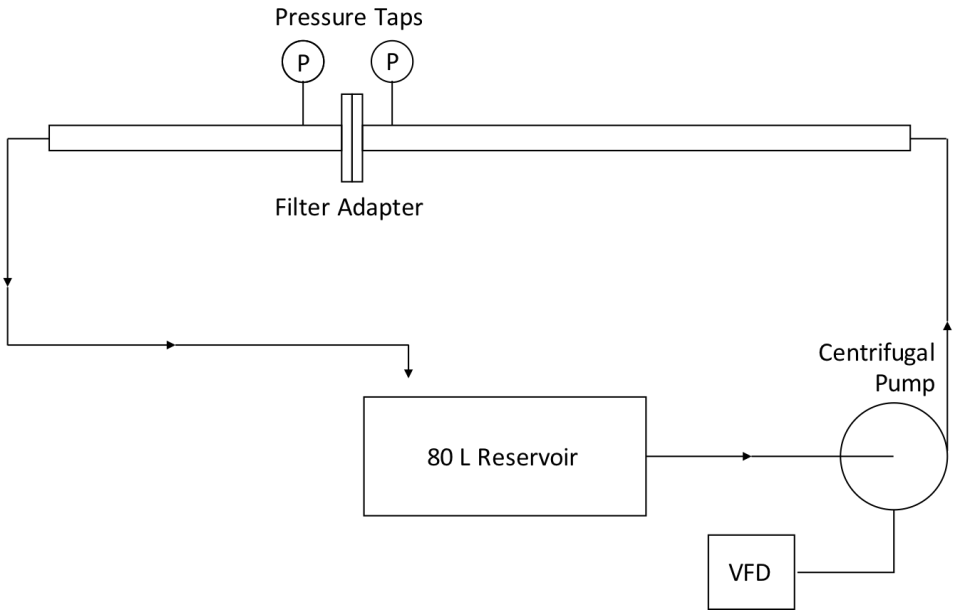

Figure 2.1: Schematic diagram of the experimental setup.

A Gould NPE 1HP pump was used to provide a consistent flow over a wide range of flow rates. The Gould NPE pump is a centrifugal pump controlled by an SMVector variable frequency drive (VFD). An OMEGA digital pressure gauge was used to measure the pressure drop across the mesh filter. The pipe diameter was constant across the mesh, such that the total pressure drop was equal to the static pressure difference across the mesh. The digital pressure gauge measures the pressure in [mbar], with an accuracy to 0.5 [mbar]. A static pressure of 1 [m] of water was tested before each experiment, to ensure proper calibration of the sensor. Each mesh filter was characterized in three complete experiments to ensure proper statistical analysis could be conducted. Table 2.1 shows a summary of the relevant specifications of the experimental apparatus.

Based on the pipe diameter, 0.041 [m], and flow velocity, 0.3 - 1.5 [m/s], the Reynolds

Table 2.1: Experiment specifications.

Component	Specification
Inlet Pipe	Length = 2.44m, Diameter = 0.041m
Outlet Pipe	Length = 1.52m, Diameter = 0.041m
Water Reservoir	80L
Velocity Range	0.3 - 1.5 [m/s]
Pump	Gould 1HP (745.7 W), centrifugal pump
VFD Controller	SMVector, 1.5HP (1118.55 W)

number based on diameter ranges from 12000 to 61000, making the flow fully turbulent (Re > 2300) [18]. The length of the pipe was selected to ensure a fully developed flow at the filter location.

Each filter was characterized for the experiment based upon two parameters; thread diameter and open area percentage. The properties of the filters for each nominal pore size are given in Table. 2.2.

Table 2.2: Geometric properties of the tested mesh filters.

Nominal Pore Size [μm]	Thread Diameter [μm]	Open Area Percentage [%]
158	145	26
350	250	34

2.4 Numerical Simulation

In order to determine the inflow characteristics for flow through the mesh filter, a numerical study was first performed on the pipe flow to determine the velocity profile and turbulence quantities experienced at the filter. Using this data, boundary conditions for a representative element of the filter were determined for a second numerical study, from which results are compared to the experimental data.

2.4.1 Mesh Filter Geometric Model

Two different mesh filters were used in this experiment with nominal pore sizes of 158 and 350 [μm], as shown in Fig. 2.2. Due to the complexity of the mesh filter being modelled, an assumption was made about the size of the domain with regards to the filter pore. When considering the size of the pores (350 [μm] for example) and assuming the pore geometry to be square, there would be approximately 2300 pores if the domain was to be the entire mesh filter insert. With this number of pores and each pore needing on average 150,000 control volumes to achieve grid independence, the simulation time would be excessive. Therefore, it is more sensible to consider a representative part of the filter.

Therefore, the mesh filter was modelled using a single, spatially periodic pore. Symmetry boundary conditions were used to replicate the effects of the surrounding pores in the mesh filter insert. This simplification reduced computational time, while still providing an accurate representation of the pressure drop that would be seen across the entire filter. When observing the filter meshes under a microscope, as shown in Fig. 2.2, it is clear that while there is a repeating pattern, there are slight geometric differences from pore to pore. However, the mesh filter geometry was idealized as square, with average dimensions obtained by taking the known thread diameter and open area percentage provided by the manufacturer. The width of the domain can be calculated, corresponding to the average pore geometry within the actual mesh. It was also assumed in the idealized geometric model that the threads are circular and that thread junctions are as shown in Fig. 2.3. While Fig. 2.2, shows that the weave type, on average, is plain weave and there are locations along the mesh filter were it appears to be twill weave. It is also shown that the mesh thread deforms when the mesh is being manufactured. Since these geometric nuances would be difficult to incorporate, it was assumed for the idealized geometry that they all average out to the geometry shown in Fig. 2.3, which shows a 3D isometric view of the mesh along with the computational domain. The width of the domain, W, in Fig. 2.3(b) is 0.3 [mm] and 0.62 [mm] for the 158 and 350 [μm] mesh, respectively.

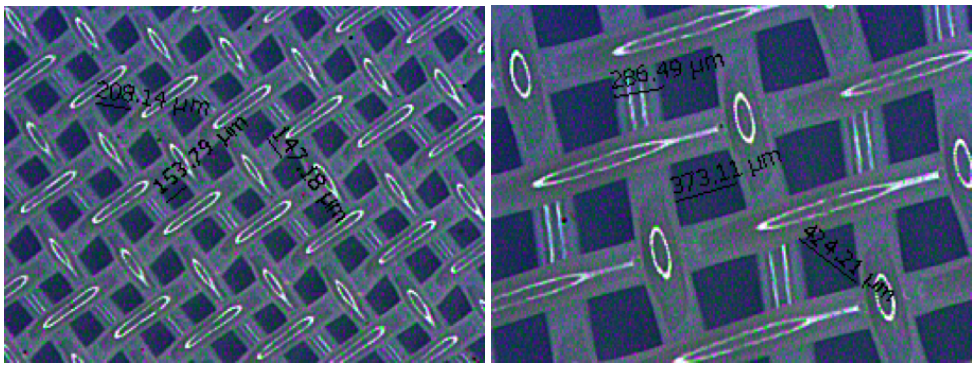

(a) (b)

Figure 2.2: Microscopic imagines of (a) 158 and (b) 350 [μm] mesh.

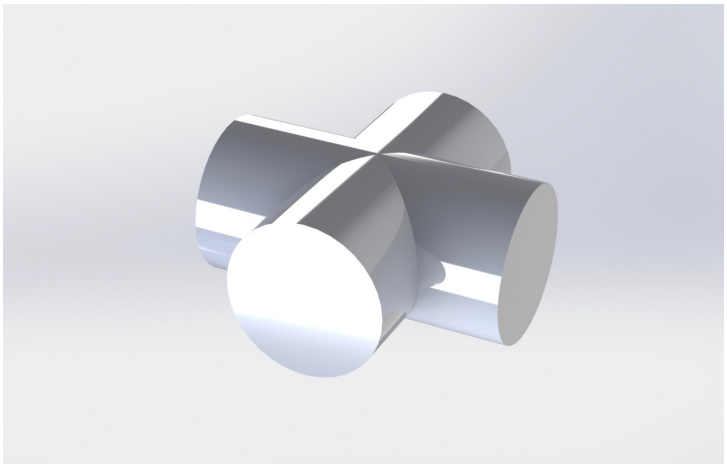

(a)

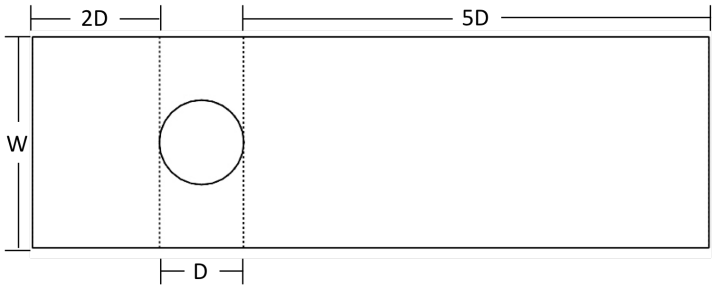

(b)

Figure 2.3: Images of (a) 3D pore model and (b) pore model computational domain.

2.4.2 Governing Equations

Conservation Equations

The inlet pipe and mesh filter models involve incompressible and Newtonian flow, therefore, the governing equations for conservation of mass and momentum are given as [19]

$$\frac{\partial}{\partial x_i}(\overline{u_i}) = 0 \tag{2.5}$$

and

$$\frac{\partial(\rho\overline{u_i})}{\partial t} + \frac{\partial(\rho\overline{u_i}\,\overline{u_j})}{\partial x_j} = -\frac{\partial\overline{P}}{\partial x_i} + \frac{\partial}{\partial x_j}(\overline{\tau_{ij}}) - \frac{\partial}{\partial x_j}\left(\rho\overline{u_i'u_j'}\right) \tag{2.6}$$

Since the flow under consideration is turbulent (pipe Reynolds numbers ranging from 12000 to 61000), $\overline{u_i}$,$\overline{u_j}$ and $\overline{P}$ denote the time-averaged velocity vectors and time-averaged pressure, respectively, u_i' and u_j' are the turbulent velocity fluctuations and $\overline{u_i'u_j'}$ denote the turbulent Reynolds stresses. The laminar stress tensor, $\overline{\tau_{ij}}$, is

$$\overline{\tau_{ij}} = \mu\left[\frac{\partial u_i}{\partial x_j} + \frac{\partial u_j}{\partial x_i}\right] \tag{2.7}$$

Turbulence Modelling

Since the flow across the filter is turbulent, a turbulence model is required. The standard k-ϵ turbulence model, with enhanced wall functions was used to model turbulence. The enhanced wall function model assures the viscosity affected, near wall region is completely resolved to the viscous sublayer. The transport equations for the k-ϵ turbulence model are given as [19]

$$\frac{\partial}{\partial t}(\rho k) + \frac{\partial}{\partial x_i}(\rho k u_i) = \frac{\partial}{\partial x_j}\left[\left(\mu + \left(\frac{\mu_t}{\sigma_k}\right)\right)\left(\frac{\partial k}{\partial x_j}\right)\right] + G_k + G_b - \rho\epsilon \tag{2.8}$$

$$\frac{\partial}{\partial t}(\rho\epsilon) + \frac{\partial}{\partial x_i}(\rho\epsilon u_i) = \frac{\partial}{\partial x_j}\left[\left(\mu + \left(\frac{\mu_t}{\sigma_\epsilon}\right)\right)\left(\frac{\partial k}{\partial x_j}\right)\right] + C_{1\epsilon}\left(\frac{\epsilon}{k}\right)(G_k) - C_{2\epsilon}\rho\left(\frac{\epsilon^2}{k}\right) \tag{2.9}$$

and the Reynolds stress term, using the Boussinesq approximation, is

$$\left(\rho\overline{u_i' u_j'}\right) = \mu_t\left[\frac{\partial\overline{u_i}}{\partial x_j} + \frac{\partial\overline{u_j}}{\partial x_i}\right] - \frac{2}{3}\rho k\delta_{ij} \tag{2.10}$$

where μ_t is the eddy viscosity, k is the turbulent kinetic energy and δ_{ij} is the Kronecker delta. The turbulent eddy viscosity is computed as

$$\mu_t = \rho C_\mu\left(\frac{k^2}{\epsilon}\right) \tag{2.11}$$

and the turbulence production is

$$G_k = \mu_t S^2 \tag{2.12}$$

The values of the turbulence constants in the above Eqs. 2.8 and 2.9 are shown in Table. 2.3, below

Table 2.3: Turbulence constants values.

$C_{1\epsilon}$	$C_{2\epsilon}$	C_μ	σ_k	σ_ϵ
1.44	1.92	0.09	1.0	1.3

The above equations were solved using the commercial CFD software ANSYS®Fluent, Release 17.2. Second order upwind discretization schemes where chosen for the transport equations and the segregated SIMPLE scheme was used for pressure velocity coupling.

2.5 Results

2.5.1 Inlet Pipe Simulations

In the idealized mesh filter model, only a single pore is being modelled. There is a turbulent kinetic energy and velocity distribution across the inlet boundary, however, these distributions are not known. To determine the correct turbulence and velocity boundary conditions for the mesh filter model, further examination of the inlet pipe flow was required.

The inlet pipe model was generated in SOLIDWORKS®, 2017 and then imported into ANSYS Workbench. The dimensions of the model are the same as in the experiment, with a length of 2.44 [m] and diameter of 0.041 [m]. Meshing was done using ANSYS Meshing and a grid independence study was done to ensure results did not change by more than 1% between subsequent grids, as shown in Table 2.4. The fine grid was used for all subsequent calculations. The discretization methods chosen can be seen in Table 2.5 and the boundary conditions used can be found in Table 2.6.

Table 2.4: Results for the grid independence test on inlet pipe for velocity and turbulent kinetic energy profiles, where coarse and fine correspond to 84375 and 159375 elements within the domain.

Radial position	**Velocity [m/s]**			**Turbulent Kinetic Energy** [m^2/s^2]		
[m]	Coarse	Fine	% Difference	Coarse	Fine	% Difference
0.00108	0.59613	0.59610	0.00005	0.00108	0.00109	0.00690
0.00538	0.58891	0.58890	0.00001	0.00123	0.00124	0.00560
0.00968	0.57349	0.57352	0.00005	0.00151	0.00152	0.00402
0.01399	0.53363	53365	0.00005	0.00205	0.00205	0
0.01829	0.45509	0.45509	0	0.00290	0.00290	0

To produce a general set of boundary conditions for the mesh filter model from the inlet pipe model, the results for the turbulent kinetic energy and velocity profiles needed to be comparable between different simulations. This was done by normalizing the turbulent kinetic energy into the turbulence intensity, which is defined as [19]

Table 2.5: Parameters and discretization schemes chosen for inlet pipe CFD model.

Category	Setting	Value
General	Solver	Pressure based, steady, absolute reference frame
Models	Energy	Isothermal
	Viscous	Turbulent (k-ϵ with enhanced wall function)
Solution Methods	Scheme	Simple
	Gradient	Least Squares Cell Based
	Pressure	Second Order
	Momentum, energy and other equations	Second Order Upwind
Residuals	Scaling	Local Scaling
	Convergence Criteria	1.0e-5

Table 2.6: CFD model boundary conditions.

Location	Boundary Condition Type	Setting	Value
Inlet	Velocity	Specified velocity magnitude, normal to boundary	Bulk velocity from experiment
	Turbulent Kinetic Energy	Specified Intensity	5%
	Eddy Dissipation Rate	Hydraulic Diameter	0.040894
Outlet	Pressure	Gauge	0
	Turbulent Kinetic Energy	Specified Intensity	5%
	Eddy Dissipation Rate	Hydraulic Diameter	0.040894
Surface of Mesh	Wall	No Slip	-
Outside of Domain	Symmetry	Symmetry	-

$$I = \frac{1}{U_{bulk}}\sqrt{\frac{2k}{3}} \tag{2.13}$$

where I is the turbulence intensity, U_{bulk} is bulk fluid velocity specified at the inlet and k is the turbulent kinetic energy. The velocity profile was normalized using the pipes bulk velocity, Eq. 2.14.

$$u^* = \frac{u}{U_{bulk}} \tag{2.14}$$

where u^* is the normalized velocity as a given location, u is the measured velocity at a given location and U_{bulk} is the bulk inlet velocity.

Figure 2.4 and 2.5 show the results of the inlet pipe CFD model. The turbulence intensity profiles are shown in Fig. 2.4. While the different dimensionless profiles do not collapse onto a single curve, it is shown that the value is generally bounded between 5% and 10%. Figure 2.5 shows that the normalized velocity profiles are the same for varying inlet velocities, which is expected (Schlichting et al. [20]).

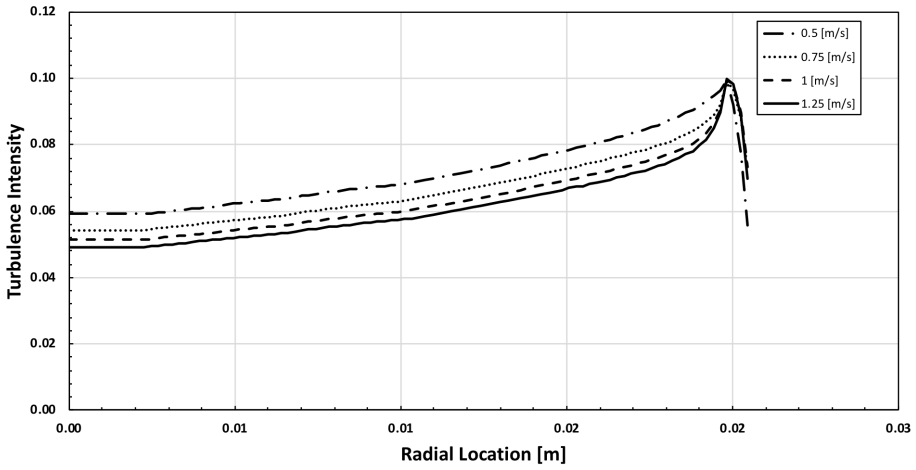

Figure 2.4: Turbulence intensity profile at pipe outlet for 4 different inlet velocities.

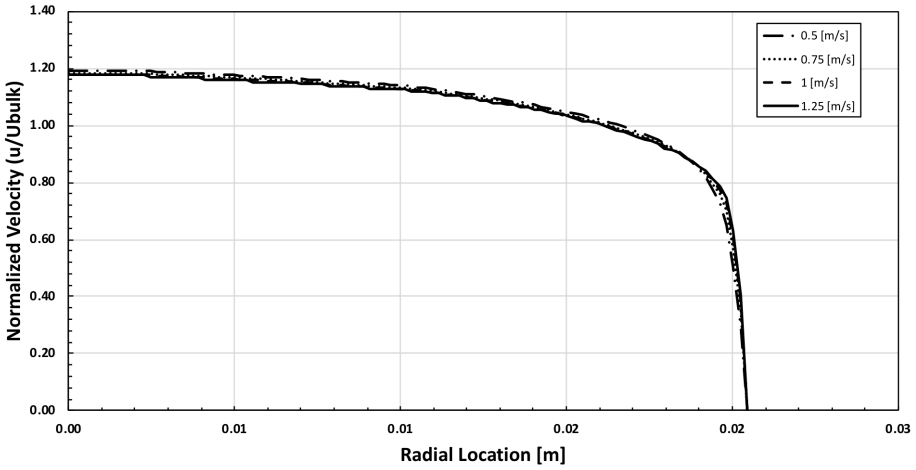

Figure 2.5: Normalized velocity profile at pipe outlet for 4 different inlet velocities.

2.5.2 Sensitivity Analysis

In the CFD model of the mesh filter, the turbulence intensity is given as a boundary condition. To test the effect of turbulence intensity on pressure drop, the turbulence intensity was varied from 1 - 10%, on the 350 [μm] mesh filter model, with 5% being the reference value. Also, a uniform velocity inlet boundary condition of 0.5 [m/s] was used for this sensitivity study. The results in Table 2.7 shows that the inlet turbulence intensity has little affect on the predicted pressure drop across the mesh filter, over the range of intensities considered. Therefore, the

inlet turbulence intensity was held constant at 5% for all subsequent calculations.

Figure 2.5, shows the normalized velocity profile varies from 0.9 - 1.2 times the bulk velocity for the majority of the pipe radius, then quickly transitions to 0 at the pipe wall. This transition range from 0.9 to 0 covers a small area and contributes little to the pressure drop across the mesh filter. Therefore, the sensitivity analysis on the inlet velocity was done by selecting a given bulk velocity from the inlet pipe CFD model, 0.5 [m/s], applying the multiplication factors from 0.9 to 1.2 to the 350 [μm] mesh filter model, and observing the computed pressure drop. Taking the results from Fig. 2.6 and comparing them to the pressure drop values gathered from experimental results, it was found that the peak velocity within the pipe (1.2 times the bulk velocity) gave the best agreement with the pressure drop measured in the experiments, which was 0.0112 [bar]. Therefore the peak velocity was used as the velocity boundary condition for all subsequent calculations.

Table 2.7: Turbulence intensity sensitivity analysis on pressure drop across mesh filter.

Turbulence Intensity	$P_{inlet} - P_{outlet}$ **[Pa]**	**% Difference**
1	5302.52	0.26
2	5304.6	0.22
3	5307.4	0.17
4	5310.8	0.10
5	5316.23	-
6	5320.87	0.09
7	5325.9	0.18
8	5331.25	0.28
9	5336.91	0.39
10	5340.47	0.46

2.5.3 Mesh Filter Experiments

Water flow experiments were run on the 158 and 350 [μm] mesh filters in triplicates. This ensured that proper statistical analysis could be done on the data to determine the average and standard deviation for a given velocity. Figure 2.7 shows the raw experimental results from the experiment and Fig. 2.8 shows the average values at a given velocity for each mesh filter type,

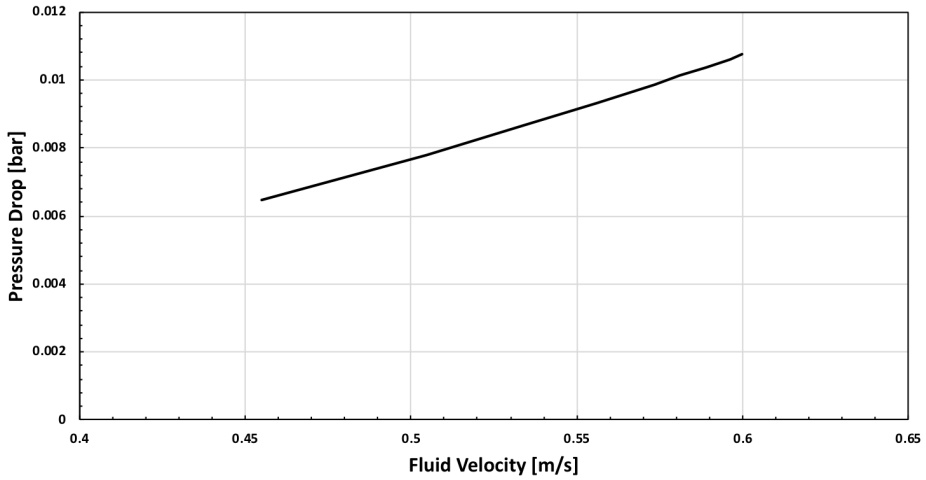

Figure 2.6: Pressure drop computed for the representative filter element as a function of the inlet boundary velocity.

along with the standard deviation. As expected, the pressure drop follows a quadratic trend with increasing fluid velocity. This confirms the flow is in the Forchheimer flow regime and should be modelled quadratically, rather than linearly.

Figures 2.7 and 2.8 show that the measured pressure drop on the 350 [μm] mesh filter values are similar for the three experimental trials, whereas measurements on the 158 [μm] mesh filter have more variability. The cause of the variability for the 158 [μm] mesh filter was assumed to be the inconsistent filter geometry. Referring back to Fig. 2.2, the variation in the filter geometry (thread diameter and pore size) is considerable, meaning that for a given filter piece, the effective pore size can change dramatically.

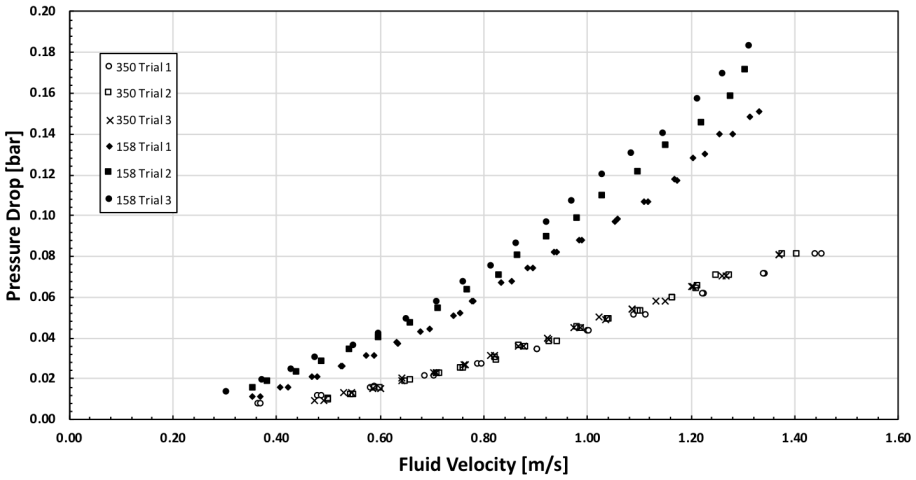

Figure 2.7: Experimental results for mesh filters with nominal pore sizes of 158 and 350 [μm].

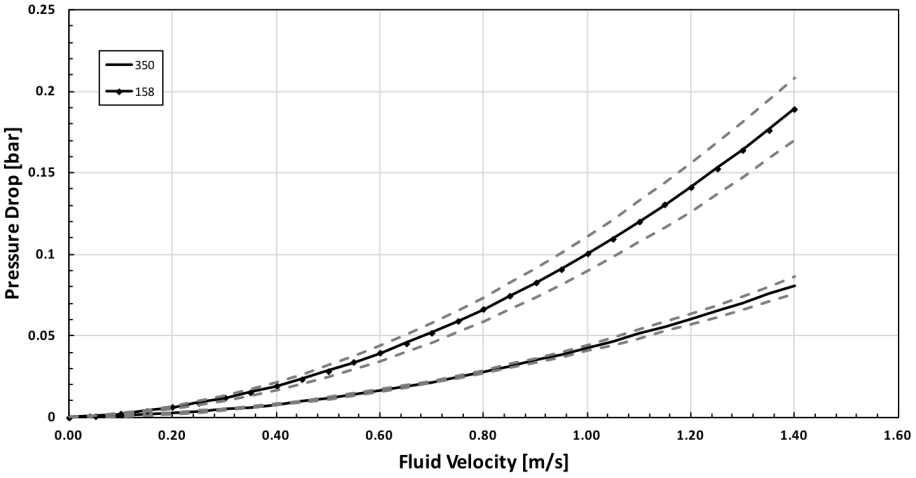

Figure 2.8: Averaged experimental results (solid lines) with dashed lines showing one standard deviation in each direction.

2.5.4 Mesh Filter Simulations

The boundary conditions and discretization solution methods for the mesh filter simulations are summarized in Table 2.8 and Table 2.9, respectively. For both the 158 and 350 [μm] mesh filter geometries, a grid independence test, proposed by Celik et al. [21], was done. The grid was refined to 1%, as seen in Table 2.10 and 2.11, for the 158 and 350 [μm] mesh filters, respectively. The fine mesh was used for both the 158 and 350 [μm] for all subsequent

calculations.

Table 2.8: Generalized boundary conditions for mesh filter CFD model.

Location	Boundary Condition Type	Setting	Value
Inlet	Velocity	Specified velocity magnitude, normal to boundary	1.2*Bulk Velocity
	Turbulent Kinetic Energy	Specified Intensity	5%
	Eddy Dissipation Rate	Hydraulic Diameter	Hydraulic diameter of entire mesh domain
Outlet	Pressure	Gauge	0
	Turbulent Kinetic Energy	Specified Intensity	5%
	Eddy Dissipation Rate	Hydraulic Diameter	Hydraulic diameter of entire mesh domain
Surface of Mesh	Wall	No Slip	-
Outside of Domain	Symmetry	Symmetry	-

Table 2.9: Parameters and discretization schemes chosen for mesh filter CFD model.

Category	Setting	Value
General	Solver	Pressure based, steady, absolute reference frame
Models	Energy	Isothermal
	Viscous	Turbulent (k-ϵ with enhanced wall function)
Solution Methods	Scheme	Simple
	Gradient	Least Squares Cell Based
	Pressure	Second Order
	Momentum, energy and other equations	Second Order Upwind
Residuals	Scaling	Local Scaling
	Convergence Criteria	1.0e-5

Table 2.10: Grid independence test for 158 [μm] mesh.

	Number of Control Volumes	Pressure Drop [Pa]
Coarse	50002	7209.55
Medium	75485	7356.66
Fine	160185	7386.1

The experimental results are compared to the CFD results for the two mesh filters in Fig. 2.9 and 2.10. It is clear that the results from the CFD analysis compare very well to the experimental values, since all CFD predictions are within one standard deviation of the experimental values. It can also be seen that the the 158 [μm] mesh filter simulations compare almost exactly to the experimental values whereas there is some difference with the 350 [μm] mesh filter. The reason for this may again be due to the variability in the pore sizes and for this case, the pores being smaller than average, thereby increasing the pressure drop. However, it is clear that even with the variability in the mesh filter, the CFD results still accurately predict the pressure drop.

Table 2.11: Grid independence study for 350 [μm] mesh.

	Number of Control Volumes	**Pressure Drop [Pa]**
Coarse	25251	1693.8
Medium	45178	1824.38
Fine	61428	1802.86

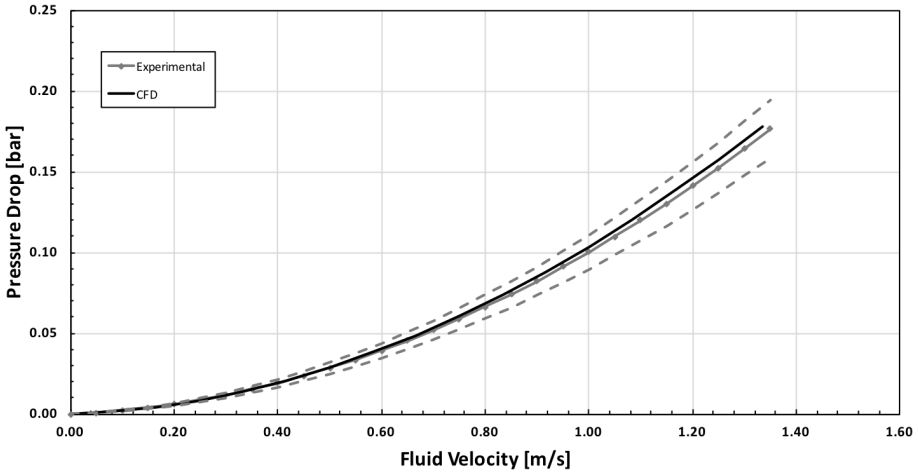

Figure 2.9: Experimental and CFD results for the 158 [μm] mesh filter, with dashed lines showing one standard deviation from experimental data.

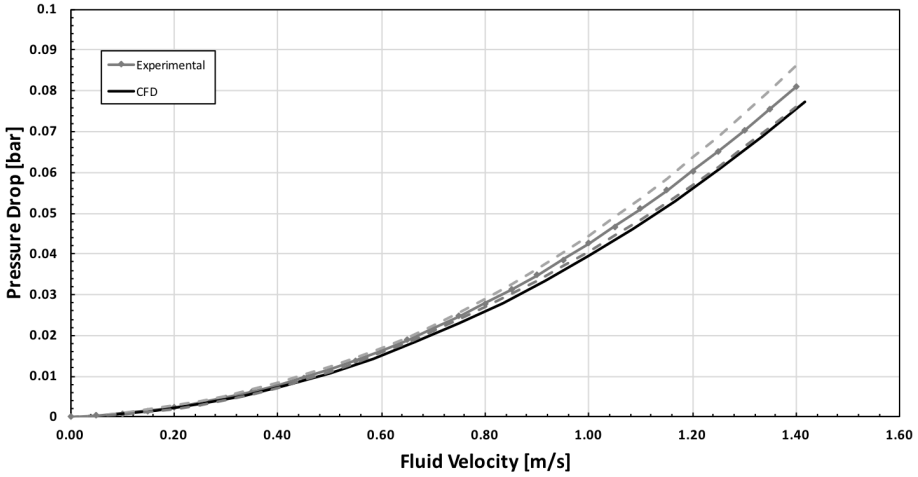

Figure 2.10: Experimental and CFD results for the 350 [μm] mesh filter, with dashed lines showing one standard deviation from experimental data.

Referring to Eq. 2.2 and substituting Eq. 2.4 for the resistance term, the resistance coefficients a and b can determined. The a and b values for the 158 and 350 [μm] mesh filters can

be found in Table. 2.12.

Table 2.12: Resistance coefficients for 158 and 350 [μm] mesh, obtained from CFD results.

Nominal Pore Size [μm]	a	b
158	1032000	9306000
350	30900	3634000

2.6 Summary

In this study, an experimentally validated numerical model was developed to characterize the resistance across mesh filters using CFD simulations of a small, idealized element of the filter. Boundary conditions for the filter element were developed by considering the flow and turbulence quantities in a fully-developed pipe flow. A sensitivity analysis revealed that the pressure drop is not significantly effected by the imposed turbulence intensity, but that the imposed velocity has a large effect. Results have shown that specifying the maximum velocity experienced by the filter as the inlet boundary condition for the filter element provides the best match with experimental data, while imposing the bulk velocity results in significant error.

Bibliography

[1] Bussière, W., Rochette, D., Clain, S., André, P., and Renard, J. B., 2017, "Pressure drop measurements for woven metal mesh screens used in electrical safety switchgears," International Journal of Heat and Fluid Flow, **65**, pp. 60–72.

[2] Kołodziej, A., Jaroszyński, M., Janus, B., Kleszcz, T., Łojewska, J., and Łojewski, T., 2009, "An Experimental Study of the Pressure Drop in Fluid Flows Through Wire Gauzes," Chemical Engineering Communications, **196**(8), pp. 932–949.

[3] Kays, W. and London, A., 1964, *Compact Heat Exchangers*.

[4] Teitel, M., 2010, "Using computational fluid dynamics simulations to determine pressure drops on woven screens," Biosyst. Eng., **105**(2), pp. 172–179.

[5] Chu, C. C. and Rawlinson, J., 1994, "Mathematical modeling of water permeability of surgical fabrics for vascular use," Journal of Biomedical Materials Research, **28**(4), pp. 441–448.

[6] Meireles, M., Prat, M., and Estachy, G., 2015, "Analytical modeling of steady-state filtration process in an automatic self-cleaning filter," Chemical Engineering Research and Design, **100**, pp. 15–26.

[7] Tien, C., Ramarao, B. V., and Yasarla, R., 2014, "A blocking model of membrane filtration," Chemical Engineering Science, **111**, pp. 421–431.

[8] Tien, C. and Ramarao, B. V., 2017, "Modeling the performance of cross-flow filtration based on particle adhesion," Chemical Engineering Research and Design, **117**, pp. 336–345.

[9] Ho, C. C. and Zydney, A. L., 2000, "A Combined Pore Blockage and Cake Filtration Model for Protein Fouling during Microfiltration," J Colloid Interface Sci, **232**(2), pp. 389–399.

[10] Salehi, E., Madaeni, S. S., Shamsabadi, A. A., and Laki, S., 2014, "Applicability of ceramic membrane filters in pretreatment of coke-contaminated petrochemical wastewater: Economic feasibility study," Ceramics International, **40**(3), pp. 4805–4810.

[11] Wang, Q. K., Matsuura, T., Feng, C. Y., Weir, M. R., Detellier, C., Rutadinka, E., and Van Mao, R. L., 2001, "The sepiolite membrane for ultrafiltration," Journal of Membrane Science, **184**(2), pp. 153–163.

[12] Wu, W. T., Liu, J. F., Li, W. J., and Hsieh, W. H., 2005, "Measurement and correlation of hydraulic resistance of flow through woven metal screens," International Journal of Heat and Mass Transfer, **48**(14), pp. 3008–3017.

[13] Vafai, K. and Tien, C., 1981, "Boundary and inertia effects on flow and heat transfer in porous media," International Journal of Heat and Mass Transfer, **24**(2), pp. 195–203.

[14] Nield, D. A. and Bejan, A., 2013, "Mechanics of Fluid Flow Through a Porous Medium," Convection in Porous Media, pp. 1–778.

[15] Skjetne, E. and Auriault, J.-L., 2014, "High-Velocity Laminar and Turbulent Flow in Porous Media," CEUR Workshop Proceedings, **1225**(August 1999), pp. 41–42.

[16] Zhu, Z., Wang, Q., and Wu, Q., 2017, "On the examination of the Darcy permeability of soft fibrous porous media; new correlations," Chemical Engineering Science, **173**, pp. 525–536.

[17] Sun, H., Bu, S., and Luan, Y., 2015, "A high-precision method for calculating the pressure drop across wire mesh filters," Chemical Engineering Science, **127**, pp. 143–150.

[18] Moran J., M., 2013, *Fundamentals Of Engineering Thermodynamics*, vol. 53.

[19] 2015, "k-ϵ Turbulence Model," ANSYS Inc., USA.

[20] Schlichting, H. and Gersten, K., 1960, *Boundary layer theory*.

[21] Celik, I. B., Ghia, U., Roache, P. J., Freitas, C. J., Coleman, H., and Raad, P. E., 2008, "Procedure for Estimation and Reporting of Uncertainty Due to Discretization in CFD Applications," Journal of Fluids Engineering, **130**(7), p. 78001.

Chapter 3

A Mathematical Model of an Rotating Belt Filter

3.1 Introduction

Increasing population size and urban expansion has increased the demand on wastewater treatment plants (WWTP), which can be seen in the amount of pollution and volume of influent wastewater [1, 2]. The pollution in wastewater is characterized by the amount of total suspended solids (TSS), oxygen-demanding materials, dissolved organic compounds, and harmful bacteria present [3]. The treatment steps for removing these pollutants are: (i) primary treatment, for suspended solids removal; (ii) secondary treatment, for the removal of biodegradable organic matter and nutrients; and (iii) tertiary treatment, for the removal of residual suspended solids and nutrients along with disinfection [4]. In this study, primary treatment is the focus.

The most common method for primary treatment in WWTPs are primary clarifiers (PC), which vary in shape, size, and numbers depending on the treatment plant's capacity, with an average diameter range of 12 [m] to 45 [m] and a common depth of 4.3 [m] [4]. They work on the premise of gravity separation where influent wastewater is supplied to a PC and particulates within the wastewater sink to the bottom of the PC during a detention time of 1.5 to 2.5 hours. The accumulated sludge on the bottom of the PC is then transfered for de-watering and

the remaining clarified water above is transferred to secondary treatment [5]. The main issue regarding PCs are their inability to naturally remove sufficient TSS from the influent wastewater. Chemically enhanced primary treatment (CEPT), where a coagulant is introduced into the influent wastewater stream to bind particulate together, is a common solution to this issue. The downfall, however, is the additional cost of the chemicals fed into the influent wastewater, along with an increased sludge production [6].

One of the technologies used to replace or augment PCs are rotating belt filters (RBF). RBFs have been found to conserve energy, reduce capital and operational costs, and provide a compact footprint [6, 7]. Also, RBF pilots have achieved TSS removal rates greater than 50% [8, 9, 10, 11], higher nitrogen removal [12] and increased energy potential of the sludge removed from the wastewater [13]. This increased removal efficiency allows for reduced energy loads in aeration tanks, increased nutrient removal and greater energy recovery in anaerobic digestion [14]. Like PCs, RBFs also allow for CEPT, which can further increase TSS removal [8, 9].

RBFs work on a dual filtration cycle where an inclined, continuously moving belt filter is used to separate particulate from the influent wastewater. The influent wastewater is gravity fed through the belt filter, where it is captured and forms a cake layer. The formation of the cake layer allows for smaller particulate to be captured through cake filtration, which can capture particulate up to three times smaller than the mesh filter pore size [15]. Due to the cake layers importance, the belt speed is usually controlled dynamically depending on the water height in the unit and the influent TSS concentration. This enables the optimal cake layer growth on the filter, allowing an optimal balance between the flow rate through the unit and the removal efficiency. At the end of each revolution of the filter, the cake layer is removed by various methods, including a physical scraper, air or water jet.

Despite their promise, few studies been carried out to characterize RBF performance [16, 17]. This is likely due to complex hydrodynamics that prevail during the filtration process as the cake layer forms on the filter. Numerous mathematical models have been presented

that characterize the resistance of mesh and cake layers [18, 19, 20, 21, 22, 23, 24, 25, 26]. These models show that the cake resistance is related to the cake porosity, particle density, particle diameter and cake solidity. They can be further applied to determine the flow rate or pressure drop across a mesh and cake layer [19, 20, 21, 23, 24]. These models, however, make assumptions that are not applicable when modeling an RBF. The main assumption made is that the flow through the cake and mesh layer are either constant flow rate or constant pressure, which is not applicable to an RBF given the continually changing water height and flow rate through the unit. Another assumption made is that the mesh resistance is a constant value. This assumption is true for low filtration rates, however, with the through flow rates RBFs are able to achieve, the mesh resistance has been observed to become linearly proportional to the velocity of water flowing through it [27]. Finally, the parameters used to calculate the cake resistance (cake porosity, particle density, particle diameter and cake solidity) are all continually changing in the RBF and are both costly and time consuming to quantify.

Rusten and Lundar [28] proposed a method for characterizing the removal efficiency and hydraulic capacity of an RBF experimentally using a gravity drainage column test. In their experiment, a cylindrical pipe holds a known volume of water above a value which controls the flow of wastewater through a mesh filter insert below. The valve is then opened and the wastewater, with a known TSS concentration, is allowed to flow through the filter. The effluent wastewater is then tested to determine the concentration of TSS from which the removal efficiency can be determined. The amount of time passed during the experiment is then used to calculate the hydraulic capacity, for a given influent TSS concentration.

The present study proposes a method that can efficiently and accurately model the hydraulic capacity and removal efficiency of an RBF. THe model can be used to conduct parametric studies of an RBF system and also as a tool to monitor and anticipate performance of working RBF systems. A column test experiment will first be modelled mathematically to compute and examine the cake growth during the filtration process. This data will then be used as an operating parameter for a generic one-dimensional RBF model. It will be shown using RBF

pilot data that the one-dimensional model can accurately predict the performance of an RBF for various operating conditions. The RBF model is then extended to include a PID controller that adjusts the RBF model operation for varying inlet boundary conditions.

3.2 Materials and Methods

3.2.1 Theory

The pressure drop across a porous medium is described by Darcy's law, given as

$$\frac{\Delta P}{L} = \frac{\mu U}{K} \tag{3.1}$$

where ΔP is the pressure differential, L is the thickness of the medium, μ is the dynamic fluid viscosity, U is the bulk fluid velocity, and K is the permeability. Equation 3.1 can also be written in terms of total flow resistance, R_T, as

$$\Delta P = \mu U R_T \tag{3.2}$$

where R_T is the total resistance across the system. Note that the length of the medium, L, is included in the resistance term given that the thickness of the cake layer is continuously varying.

There are two issues that arise using this formulation. First, by combining the cake and mesh resistance, there is no ability to accurately model fluctuations in cake resistance – caused by varying influent TSS concentrations – without also changing the mesh resistance. Second, considering mesh resistance to be a constant value is only applicable for low Reynolds number flows (Re <1). With higher velocity flows, the mesh resistance goes through a transitional regime then into the Forchheimer flow regime, where the resistance to fluid flow is linearly proportional to the fluid velocity [27, 29, 30]. To allow the model to accurately account for changes in influent TSS concentrations and changes in mesh resistance due to varying fluid

velocity, the total resistance, R_T, will be modelled as $R_T = R_{mesh} + R_{cake}$ where the mesh resistance term, R_{mesh}, can also be shown as

$$R_{mesh} = a + bU \tag{3.3}$$

where a and b are resistance constants for a given mesh type.

Thus, the final form of Darcy's law used in the proposed model is formed by applying the total resistance formulation and mesh resistance terms from Eq. 3.3, to Eq. 3.2, to give:

$$\Delta P = \mu U \left[(a + bU) + R_{cake}\right] \tag{3.4}$$

3.2.2 Gravity Drainage Test

A schematic diagram of the column test apparatus is shown in Fig. 3.1. A column test is done to determine how cake resistance changes throughout the filtration cycle in an RBF. The experiment is performed by first pouring a known volume of wasterwater, with a known TSS concentration, into the column, with the valve closed. The valve is then opened and the water is allowed to flow through the filter insert. During the experiment, a sensor tracks the height of the water in the column as it changes over the course of the experiment. After all the water has passed through the filter or the filter becomes clogged, the valve is closed and the sensor stopped.

It has been observed that the column water height follows a double exponential profile with respect to time, given as

$$h(t) = Ae^{-\alpha t} + Be^{-\beta t} \tag{3.5}$$

where A, α, B, and β are model constants that can be optimized for a given column test. At $t = 0$, the initial water height, h_0, is equal to $A + B$. Eq. 3.5 can therefore be written as

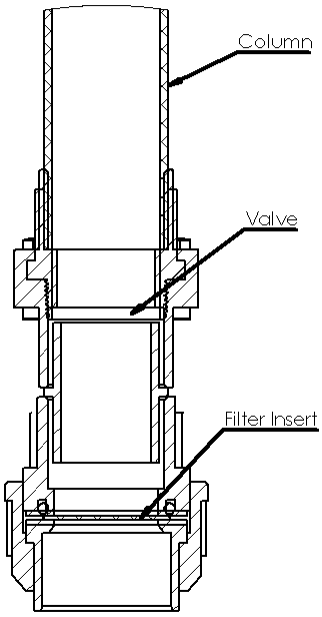

Figure 3.1: Schematic diagram of a gravity drainage column test.

$$h(t) = Ae^{-\alpha t} + (h_0 - A)e^{-\beta t} \tag{3.6}$$

Equation 3.6 can be interpreted as the sum of two sources of resistance; the first term corresponding to the mesh dominated resistance and the second corresponding to cake dominated resistance, with a transition region in between. The parameters A, α, and β are obtained by fitting column data to Eq. 3.6.

The double exponential formulation allows for a significant amount of information to be gained from the column test experiment. The fluid velocity can be calculated analytically by differentiating Eq. 3.5 with respect to time, shown as

$$U(t) = -\frac{dh}{dt} = A\alpha e^{-\alpha t} + (h_0 - A)\beta e^{-\beta t} \tag{3.7}$$

Note that the negative sign is due to the water height reducing over time. The velocity can then be used to calculate the mesh resistance from Eq. 3.3. Knowing the mesh resistance then

allows the cake resistance to be calculated by rearranging Eq. 3.4, shown as

$$R_{cake}(t) = \frac{\rho g \Delta h(t)}{\mu U(t)} - R_{mesh}(t) \tag{3.8}$$

where the head, $\Delta h(t)$, is referenced from the filter, making it equal to the instantaneous column test water height.

The cumulative filtered volume can be calculated by integrating the flow rate per unit area through the filter, with respect to time, the result of which is

$$V(t) = A\left[1 - e^{-\alpha t}\right] + (h_0 - A)\left[1 - e^{-\beta t}\right] \tag{3.9}$$

The cake resistance can then be calculated for a given cumulative filtered volume using Eqs. 3.8 and 3.9. This information will be used as an operating condition for the RBF mathematical model.

3.2.3 Sieve Test

A schematic diagram of the sieve test experimental apparatus is shown in Fig. 3.2. A sieve test is performed to understand how increasing the amount of wastewater filtered effects the removal efficiency, measured by the effluent TSS concentration. To perform a sieve test, a known volume of wastewater, with a known TSS concentration, is poured over a filter. A vacuum is used during the experiment to ensure all of the wastewater is filtered by the mesh. After all the water is filtered, the TSS concentration of the filtered effluent is determined. The experiment is then repeated for increasing volumes of water.

The sieve test results are modelled using an decreasing exponential formulation, shown as

$$C_{TSSout} = C_0 e^{-\gamma V} \tag{3.10}$$

where C_{TSSout} is the effluent concentration of TSS, V is the filtered volume per unit area and

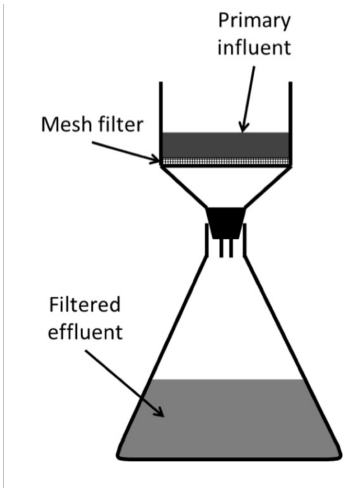

Figure 3.2: Schematic diagram of a sieve test experimental apparatus.

C_0 and γ are constants that can be calculated for a given sieve test.

3.2.4 RBF Model

A schematic of a generic RBF is shown in Fig. 3.3. Influent wastewater enters the domain to the left of the filter, at a height of $h_{upstream}$. The wastewater is then gravity fed through the filter, which is at an angle, θ, from the horizontal. Past the filter, the water travels downstream, at a height $h_{downstream}$, which is dictated by the height of the downstream weir, h_{weir}, and the flow rate through the RBF unit.

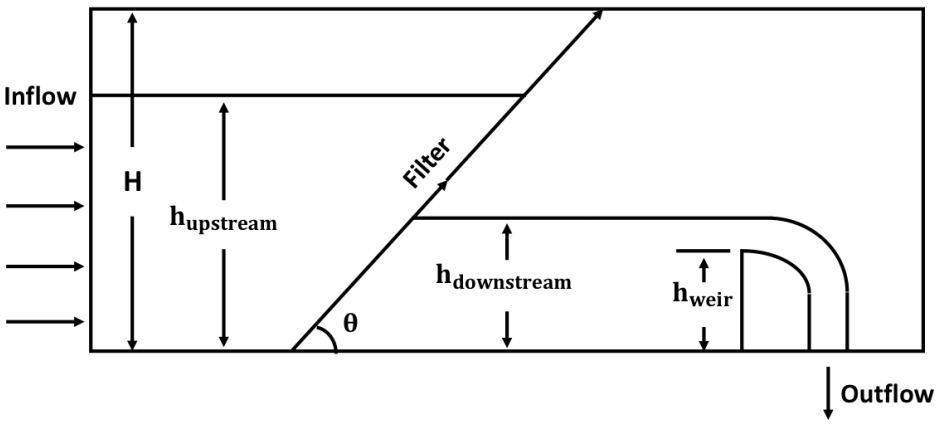

Figure 3.3: Schematic diagram of a generic rotating belt filter system.

A flow chart of the solver is shown in Figure 3.4. The RBF is modelled one-dimensionally

along the filter which is discretized into a user defined number of control volumes, an example of which can be seen in Figure 3.5. The centroids of the control volumes are denoted by x_i, where i ranges from 1 to N, where N is the total number of control volumes along the filter. The control volume's face locations, $x_{i-1/2}$ and $x_{i+1/2}$, are used in the calculation of the open area factor, β, which accounts for the potential support structure along the filter, as shown in Fig. 3.6. The open area percentage, β, varies from 0 to 1 where 0 corresponds to the entire control volume being blocked by the support structure and 1 corresponds to no blockage due to the support structure.

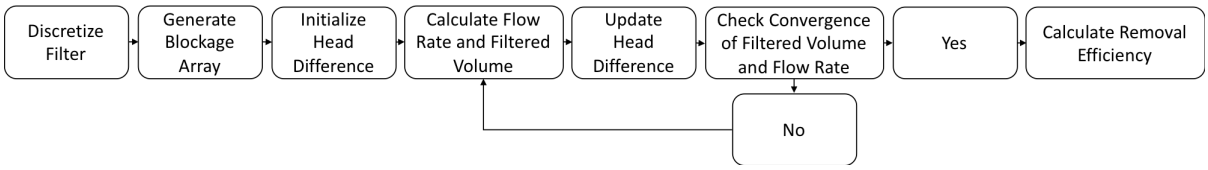

Figure 3.4: Flow diagram of one-dimensional RBF model.

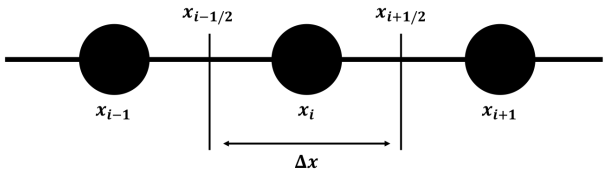

Figure 3.5: Example of a one-dimensional control volume.

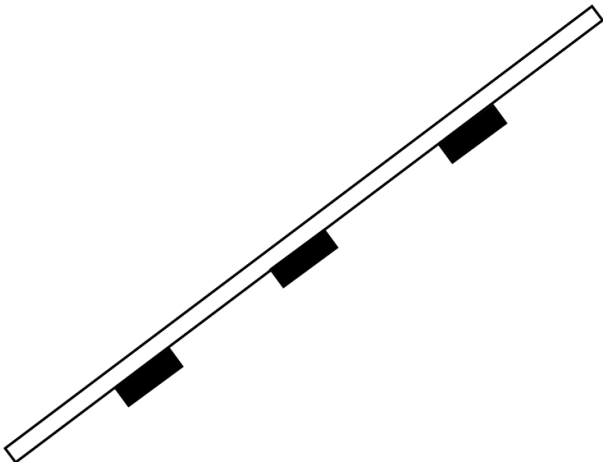

Figure 3.6: Schematic diagram showing the support structure for the filter.

The difference in hydrostatic head pressure at each volume's centroid is then calculated using the following criterion

$$\Delta h(i) = \begin{cases} h_{upstream} - h_{downstream} & \text{if } h(i) < h_{downstream} \\ h_{upstream} - h(i) & \text{if } h(i) \geq h_{downstream} \end{cases} \tag{3.11}$$

where Δh is the head difference, and $h(i)$ is the height of the filter volume. The downstream water height is a summation of the weir height and the height of water flowing over the weir, h_{above}, shown as

$$h_{downstream} = h_{weir} + h_{above} \tag{3.12}$$

where h_{above} is calculated using the following correlation, obtained from previous CFD calculations, shown as

$$h_{above} = \left[\frac{Q}{3800}\right]^{2/3} \tag{3.13}$$

where Q is the instantaneous flow rate through the system. When initializing the head difference array, the flow rate through the system is set to zero.

The code then enters a convergence loop. First, the fluid velocity through each element along the filter is calculated by rearranging Eq. 3.4, shown as

$$v(i) = \frac{-(a + R_{cake}) \pm \sqrt{(a + R_{cake})^2 - 4b(\Delta h/\mu)}}{2b} \tag{3.14}$$

where the positive root is taken to be the correct velocity. Note that for the first element of the filter, the cake resistance is assumed to be zero. The amount of volume that has been filtered through each filter element, per unit area, can be calculated by

$$V(i) = \frac{\beta v(i) \Delta x}{c} \tag{3.15}$$

where c is the linear belt speed and Δx is the length of the elemental volume. Finally flow rate per unit width through each filter element can be calculated using Darcy's law, Eq. 3.4, by isolating the velocity term, shown as

$$q(i) = \frac{\beta(i) \rho g \Delta h(i)}{\left[\mu \left(R_{cake}(i) + R_{mesh}(i)\right)\right]} \tag{3.16}$$

where for the first filter element, the cake resistance is assumed to be zero. For subsequent filter elements, the cumulative filtered volume from the previous element can be used to calculate the cake resistance term. A look up table approach is implemented, where the cumulative filtered volume at each elemental volume along the filter is compared to a table of cake resistance versus cumulative filtered volume values, generated from the column test model. If the filter element's cumulative filtered volume lies between two known values, the cake resistance is linearly interpolated between them.

The cumulative filtered volume per unit area through the entire filter can be calculated by summing the filtered volume through each filter element, shown as

$$V = \sum_{i=0}^{N-1} \frac{\beta(i) v(i)}{c} \Delta x \tag{3.17}$$

The flow rate per unit width through the entire filter can be calculated by integrating the flow through each filter volume, shown as

$$\frac{Q}{w} = \int_0^L \frac{\beta(x) \rho g \Delta h(x)}{\left[\mu \left(R_{cake}(x) + R_{mesh}(x)\right)\right]} dx \approx \sum_{i=0}^{N-1} \frac{\beta(i) \rho g \Delta h(i)}{\left[\mu \left(R_{cake}(i) + R_{mesh}(i)\right)\right]} \Delta x \tag{3.18}$$

With the overall flow rate through the system calculated, the head difference is then updated, since this changes the water height above the weir. A convergence test is then done on the cumulative filtered volume and flow rate through the system. If either does not reach a

convergence criterion of 10^{-5}, the solver recalculates the the cumulative filtered volume and flow rate using the updated head difference values.

Once the solution has converged, the cumulative filtered volume can then be used to calculate the removal efficiency using the exponential formulation derived from the sieve test experiment; with C_0 and γ values corresponding to the influent TSS concentration.

3.2.5 TSS Scaling

The benefit of separating the mesh and cake resistance terms in Darcy's law, Eq. 3.4, is the ability to scale the cake resistance for varying influent TSS concentrations. TSS scaling is done by introducing a scaling factor, τ, which is calculated by dividing the influent TSS concentration by the TSS concentration in the column test. The scaling factor, τ, can then be applied to the cake resistance versus the filtered volume curve generated from the column test.

To correctly account for a change in cake resistance, the filtered volume array is divided by τ. In Fig. 3.9, the cake resistance reaches a maximum value, consistent among column test experiments. By increasing or decreasing the TSS concentration, assuming the same particle size distribution, the result would be that the maximum cake resistance will be reached with more or less filtered volume, respectively. For example, by doubling the influent TSS concentration, the maximum cake resistance will be reached in half the filtered volume.

3.2.6 PID Controller

To control the upstream hight in a RBF unit, the belt speed is controlled dynamically using a PID controller. The general form of a PID controller equation is given as [31]

$$u(t) = k_P e(t) + k_I \int_{t_0}^{t} e(\tau)d\tau + k_D \dot{e}(t) \tag{3.19}$$

where $u(t)$ is control signal, k_P is the proportional gain, k_I is the integral gain, k_D is the derivative gain, and $e(t)$ is the control error. The control error is the difference between the process

variable, PV, and the set point, SP, shown as

$$e(t) = SP - PV(t) \tag{3.20}$$

In an RBF, the process variable in the upstream water height. The upstream water height in the system can be calculated through a mass balance, shown as

$$\Delta V = (Q_{in} - Q_{out})\Delta t \tag{3.21}$$

where ΔV is the change in volume, Q_{in} and Q_{out} are the flow rates in and out of the unit, respectively, and Δt is the time step. Figure 3.7 shows the geometry of an RBF prior to the filter which can be used to determine the change in volume in the unit, as follows

$$\Delta V = \Delta H l w \tag{3.22}$$

where ΔH is the change in water height, l is the horizontal length of the fluid and w is the width of the RBF. The fluid length, l, can be determined using the angle the filter makes with the vertical and the water height from the previous time step, shown as

$$l = H^{i-1} tan(\theta) \tag{3.23}$$

The change in height from Eq. 3.22, can then be determined as

$$\Delta H = \frac{(Q_{in} - Q_{out})\Delta t}{H^{i-1} tan(\theta) w} \tag{3.24}$$

The new water height can then be found by adding the change in height to the water height from the previous time step. The assumption that the change in volume was rectangular rather than trapezoidal is a first-order approximation which reduces the complexity of the solution. A trapezoidal volume would result in a quadratic function to determine the change in water height, where there is no clear method to determine which root is correct. With a small enough

time step, the change in volume, comparing the rectangular to a trapezoidal volume, would be nearly identical.

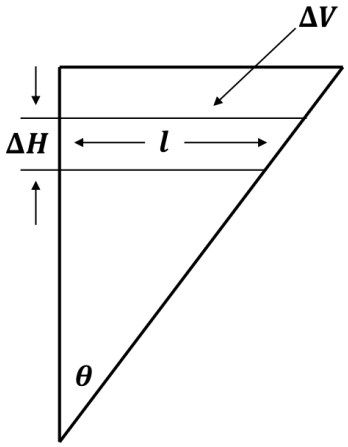

Figure 3.7: Schematic diagram showing the geometry of the RBF unit before the filter.

3.3 Results and Discussion

3.3.1 Wastewater Characteristics

The gravity drainage column test and sieve test are used as operating parameters for the RBF model as they provide necessary information on cake layer formation and resistance as well as removal efficiencies for a given influent TSS concentration. Sample column and sieve tests are shown, however, to get the most accurate predictions, column and sieve tests must be done at the site being modelled for various water qualities.

Column Test Results

Figure 3.8 shows how the water level in the column changes during over the course of the experiment. The fast initial drop in water height is due to the mesh dominated filtration. As the cake layer builds, the rate of change of water height decreases as the cake layer grows. The result of fitting the double exponential formulation (parameter values shown in Appendix 1, Case 1) is shown in Fig. 3.8. The column test was done with municipal wastewater with

a TSS concentration of 373 [mg/L]. The double exponential shows close agreement in height prediction during the course of a column test when compared to the experimental data.

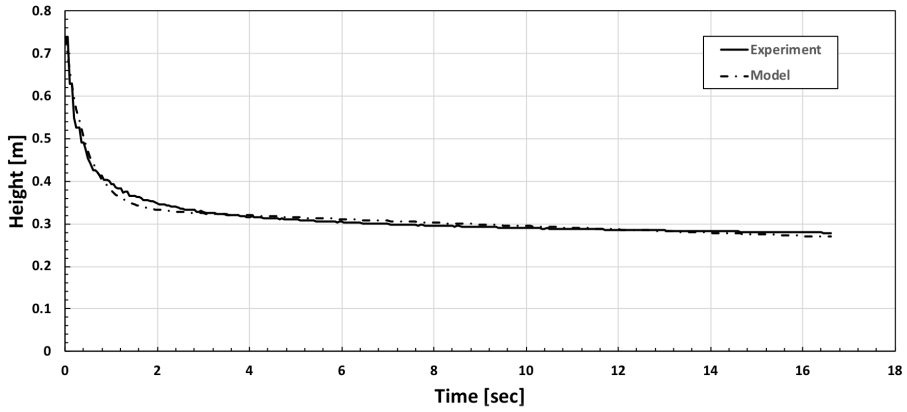

Figure 3.8: Experimental column test fitted with double exponential equation.

The cake resistance as a function of the cumulative filtered volume, per unit area, can then be calculated using Eqs. 3.8 and 3.9, as shown in Fig. 3.9.

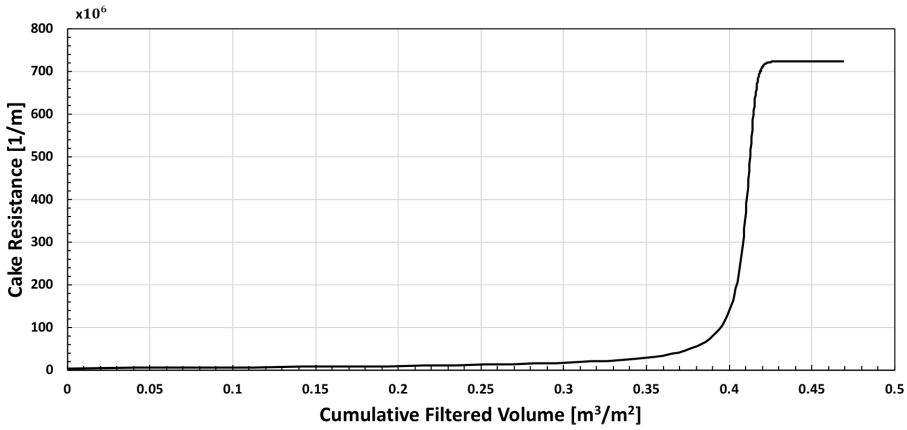

Figure 3.9: Cake resistance versus filtered volume for a column test.

The results from Fig. 3.9 are then used in the the RBF model to calculate the cake resistance for a given cumulative filtered volume along the belt. The benefit of using the column test to generate cake resistance data is the results give an overall description of cake formation and resistance without the need to determine specific characteristics of cake layer, such as the particle size distribution and cake porosity. This dramatically reduces the complexity of the experimental apparatus and model, without reducing accuracy.

Sieve Test Results

The results of a sieve test are shown in Fig. 3.10. With an increase in filtered volume, it can be seen that the effluent TSS concentrations decreases dramatically, caused by the formation of a larger cake layer on the filter. The result of fitting the exponential formulation can be seen in Fig. 3.10 where the of the sieve test fitting parameters are shown in in Appendix 1, Case 2. The sieve test was done with municipal wastewater with a TSS concentration of 202 [mg/L]. The single exponential shows close agreement between experimental results and mathematical predictions of effluent TSS concentrations.

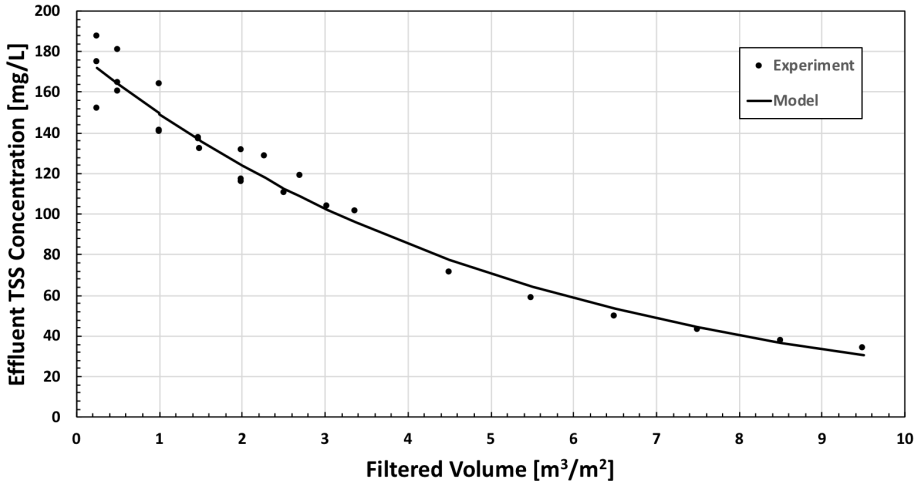

Figure 3.10: Experimental sieve test data fit with exponential formulation.

The results from Fig. 3.10 show the importance of the cake layer on removal efficiency. As the cake layer increases, the removal efficiency increases substantially. Also, like the column test, the sieve test is a very effective experiment that gives an overall understanding of the cake layer and its removal properties without the need of a complex testing apparatus.

3.3.2 RBF Model Results

The RBF code allows for the prediction of both capacity and removal efficiency for various RBF units based on the column and sieve test inputs and an influent TSS concentration of 300

[mg/L]. The values of the column and sieve test parameters are shown in Appendix 1, Case 3. Figures 3.11 and 3.12 show the capacity and removal efficiency, respectively, for four different RBF units. Table 3.1 gives the specifications of the four units being modelled.

Table 3.1: Specifications for four arbitrary RBF units.

	Height [m]	**Weir Height [m]**	**Width [m]**	**Belt Angle [°]**
Unit 1	0.3	0.1	1	30
Unit 2	0.5	0.2	1	30
Unit 3	0.7	0.3	1	30
Unit 4	0.9	0.5	1	30

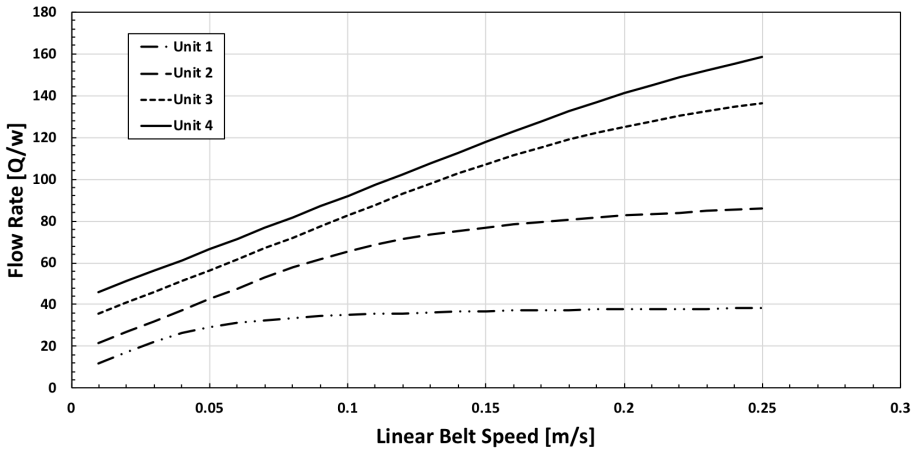

Figure 3.11: Capacity curves for RBF units of varying length, width and belt angle.

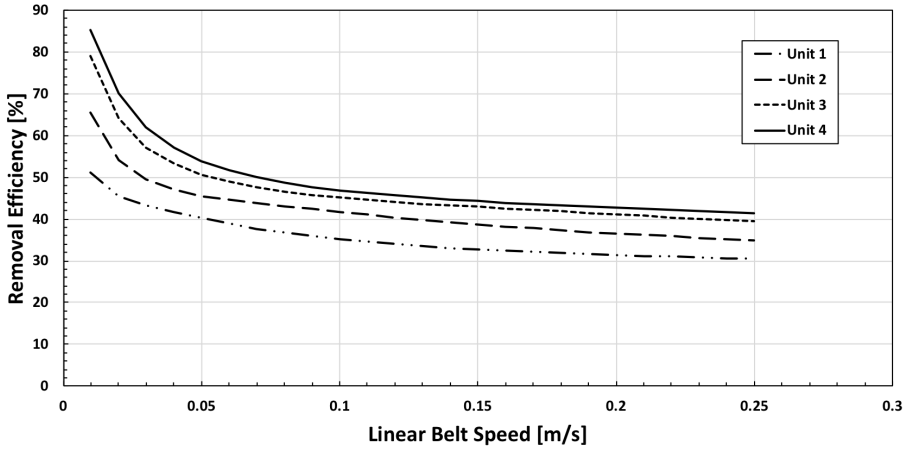

Figure 3.12: Removal curves for RBF units of varying length, width and belt angle.

Three observations can be drawn from these results. First, the flow rate capacity is higher for larger RBF units. This is expected, given the larger filter area. Second, for higher belt speeds, the flow rate capacity for a given unit increases and the removal efficiency decreases. The increased belt speed reduces the filtration cycle time and therefore reduces the size of the cake layer on the filter. The smaller cake layer is less restrictive on flow, however, limits the effectiveness of the cake layer on particle retention. The third observation is the variation in removal efficiency between the four units. The increased belt length in Units 2-4 increases the filtration cycle time, allowing a greater amount of of fluid to be filtered. This increases the cake layer thereby increasing the removal efficiency.

3.3.3 TSS Scaling Results

Figures 3.13 and 3.14 show the effect on increasing and decreasing the influent TSS concentration, from a reference value of 300 [mg/L], on RBF capacity and removal efficiency, respectively. The values for the column and sieve test parameters used are shown in Appendix 1, Case 3. As the influent TSS concentration varies, it has a large effect on the resulting capacity and removal efficiency predictions. Increasing the influent TSS concentration reduces the capacity and increases the removal efficiency of the RBF unit. This is caused by the faster growing cake layer on the filter. When the influent TSS concentration is reduced, the capacity increases and the removal decreases, caused by the reduction in cake layer growth. Given the effect that TSS scaling has on RBF performance, all subsequent calculations include TSS scaling.

3.3.4 PID Results

A study was done under steady state conditions on the gain and time step values, to observe their effect on response and settling time. The optimal gain and time step values determined can be found in Table. 3.2 and the values of the column test parameters in Appendix 1, Case 4. The k_D gain value was set to zero, as it induced significant instability. The results of starting the controller at an arbitrary initial belt speed and water height can be seen in Fig.3.15 and

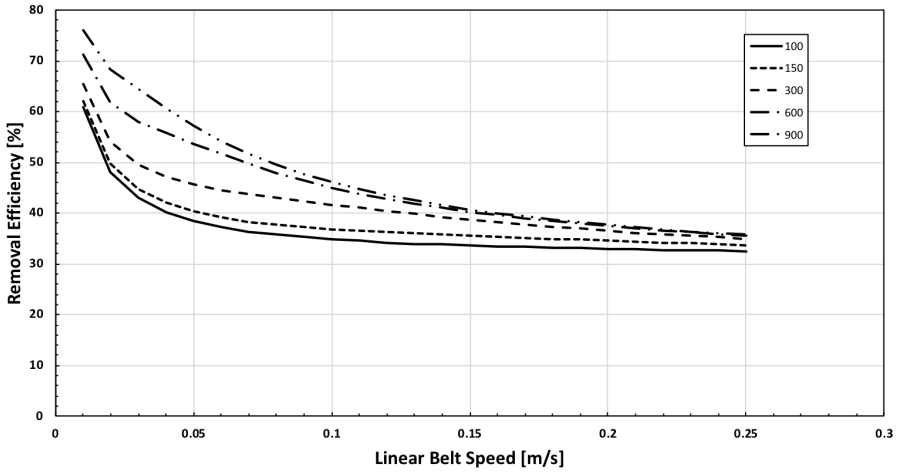

Figure 3.13: Variation in flow rate caused by varying influent TSS concentrations.

Fig.3.16, for the belt speed and height, respectively.

Table 3.2: Optimized gain and time step values.

k_p	k_I	k_D	Δt
1	0.5	0	0.5

To observe the transient response of the optimized gain and time step values, an experiment was done by varying the influent TSS concentration into the model and observing the predicted change in belt speed and upstream water height. A triangle wave form of influent TSS, ranging linearly from 150 - 650 [mg/L] over eight minutes and an inlet flow rate of 18 [L/s] was chosen as inlet boundary conditions, due to their close relation to inlet conditions experience at the pilot installation. A 0.4 [m] upstream water height was set as the operating goal. The results for PID's response in belt speed and resulting upstream height can be seen in Fig. 3.17 and Fig. 3.18, respectively.

The results show that the belt speed follows the same trend as the influent TSS concentration; linearly increasing and decreasing in accordance to the changing influent TSS concentration, maintaining the upstream water height at the set value. This shows that the gain and time step values chosen are acceptable and can be further applied in the prediction of full scale, dynamic, RBF performance.

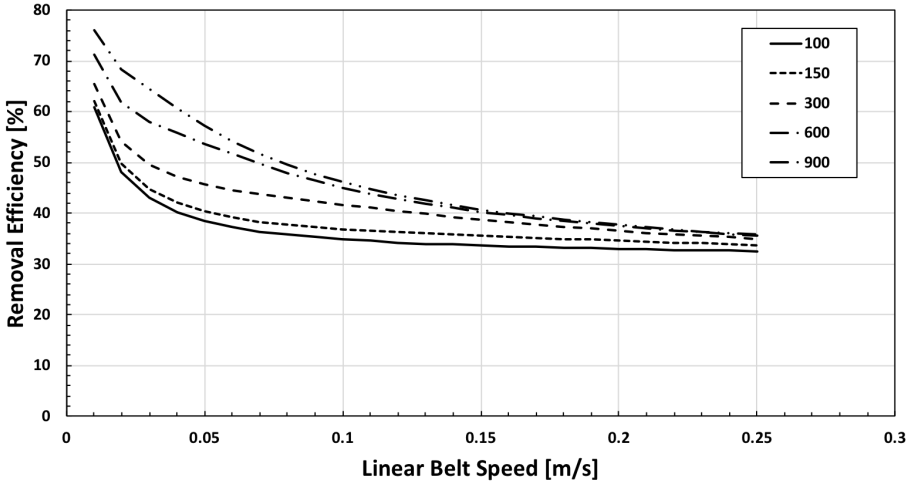

Figure 3.14: Variation in removal efficiency caused by varying influent TSS concentrations.

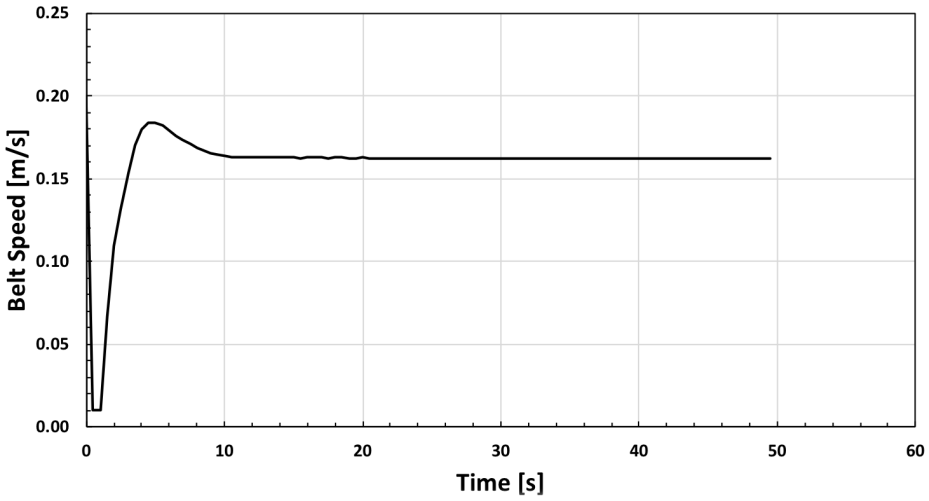

Figure 3.15: Belt speed response and settling time from an arbitrary initial belt speed.

3.3.5 Parameter Optimization

The RBF model can be verified by taking pilot unit dimensions and operating parameters (upstream water height, belt speed, and influent TSS concentration) as model inputs and comparing the predicted flow rate from the model to that of the pilot. The column test parameters and TSS values can be found in Appendix 1, Case 5 and the influent TSS concentration from the pilot data ranged from 280 - 686 [mg/L] with a mean of 442 [mg/L]. The result of this are shown in Fig. 3.20. It can be seen that there is a discrepancy between predicted and actual flow

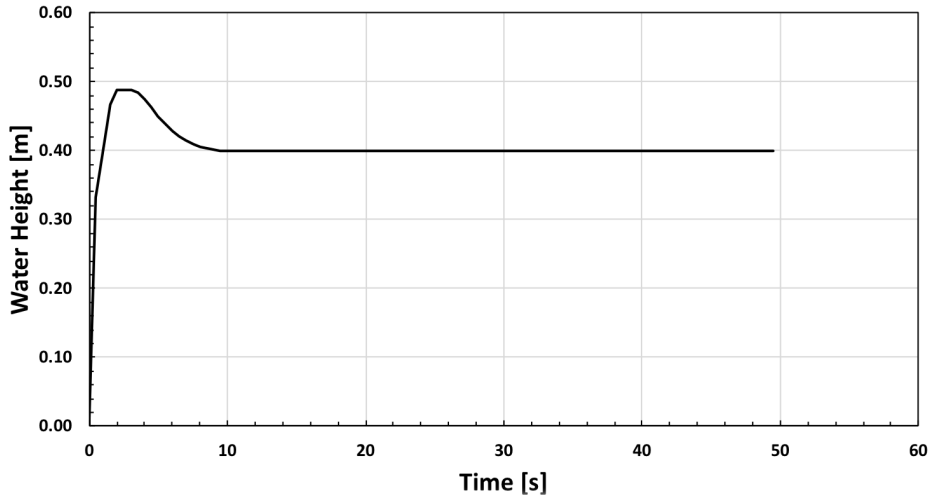

Figure 3.16: Water height response and settling time from an arbitrary initial height.

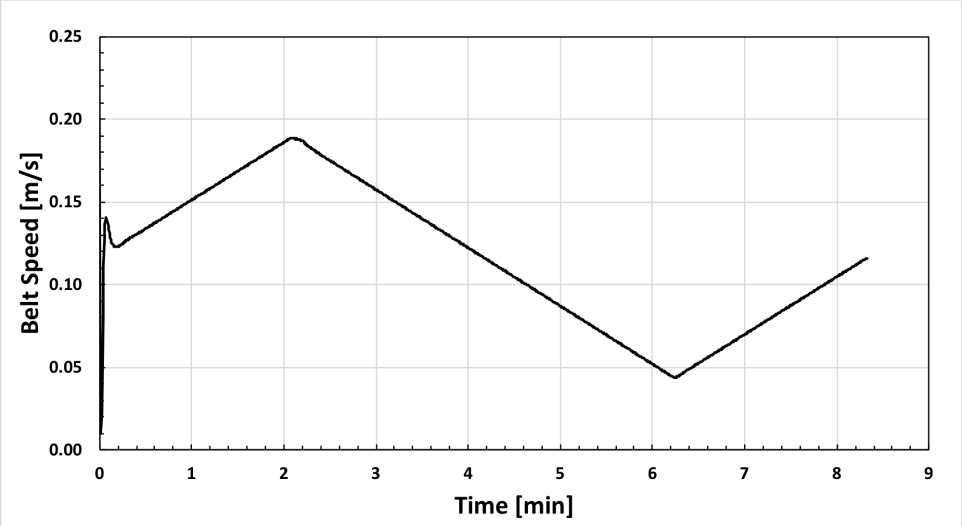

Figure 3.17: Belt speed response to a varying influent TSS concentration.

rates seen in the pilot installation.

To understand the source of this disagreement, a sensitivity analysis was done on the three sizing parameters from the column test (A, α, and β), the value of which can be found in Appendix 1, Case 6. Each parameter was varied by ± 10% and the resulting flow rates were compared. The upstream water height and belt speed were taken from pilot data with TSS values ranging from 375 - 790 [mg/L] with a mean of 638 [mg/L]. It was found that varying A had the greatest effect on RBF model performance, as seen in Figure 3.19. This result is

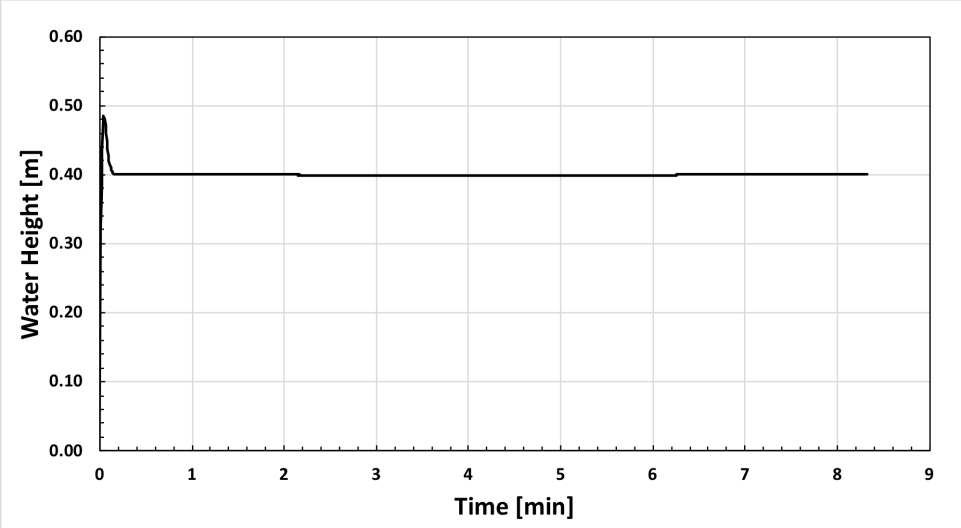

Figure 3.18: Water height response to a varying influent TSS concentration.

expected given that A dictates both the amount of mesh filtration and the transition from mesh to cake resistance in the model.

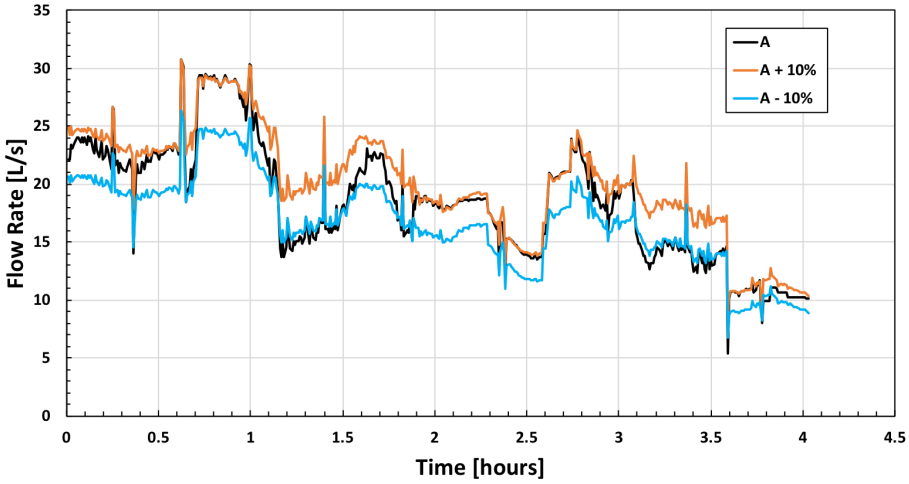

Figure 3.19: Sensitivity analysis done by varying the A parameter by ± 10%.

3.3.6 Parameter Optimization Results

An optimization was done on the A parameter to determine the physical cause of the error between predicted and pilot flow rates. The upstream water height and belt speed were taken from pilot data with TSS values ranging from 280 - 686 [mg/L] with a mean of 442 [mg/L].

The cake resistance versus filtered volume look up table was generated from a column test done on on the same day with the same wastewater as the pilot, the values of which can be found in Appendix 1, Case 5. The *A* parameter was optimized against 12.5 hours of pilot data and the resulting column test parameters can be found in Appendix 1, Case 7.

The results from the *A* optimization are shown in Fig. 3.20. The effect of optimizing *A* to pilot data is clear; where the original column test parameters under predict pilot capacity, the optimized *A* capacity predictions follows very close to that of the pilot data. From this result, two theories regarding the the error between predicted and actual capacity were generated. Under-predicting pilot capacity could be caused by the destruction of the cake layer in the pilot, caused by the turbulent inlet flow and recirculation zones along the belt. The result of this is lower cake resistance, and therefore a higher capacity when compared to the RBF model which assumes no cake destruction during the filtration cycle. It has also been found that the RBF model can over predict pilot capacity, which may be caused by imperfect cleaning of the filter in the pilot. During the calculation of the filtered volume and flow rate in the RBF model, an assumption was made that the cake resistance was zero for the first filter element, however, during the cleaning process of the filter, the cleaning mechanisms may not remove all of the cake from the filter. This would result in a greater flow restriction in the pilot and would lead to the model overpredicting the flow rate capacity.

By optimizing the *A* parameter, the two theories regarding the error in predicted pilot capacity can be accounted for. By increasing the value of *A*, the destruction of cake layer during the filtration process is accounted for by reducing the cake resistance during the filtration cycle, increasing the predicted capacity. By reducing the value of *A*, the imperfect cleaning of the filter is accounted for by increasing the amount of cake resistance in the model, reducing the predicted capacity. This optimization therefore allows for complex interactions between the wastewater and cake layer along with imperfect filter cleaning to be characterized through the change of a single input parameter, resulting in accurate prediction of true pilot performance.

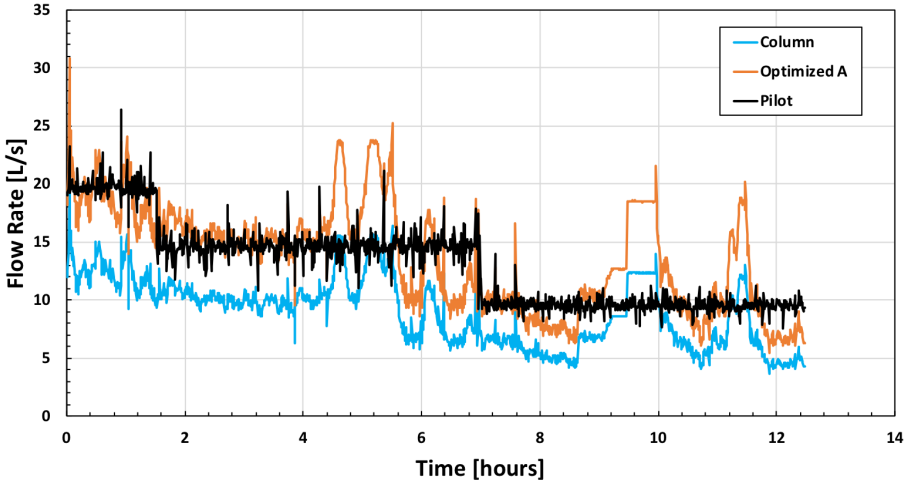

Figure 3.20: Optimized column test parameter A compared to regular data against pilot data.

3.4 Summary

In this study, an experimentally validated, one-dimensional RBF model was developed to characterize the flow rate capacity and removal efficiency of an RBF unit. Cake formation along the filter was determined by mathematically modeling a gravity drainage column test with a double exponential formulation. This formulation was then applied to Darcy's law to characterize the cake resistance for a given filtered volume of fluid. The removal efficiency was determined by mathematically modeling a sieve test. The sieve tests results gave an effluent TSS concentration for a given filtered volume, for a known influent TSS concentration. These were then used as operating parameters for a one dimensional RBF model, from which flow rate capacity and removal efficiency curves were generated for four RBF units. The model was then extended to include TSS scaling, a PID controller and parameters optimization. These extensions allows for the RBF model to accurately predict RBF pilot performance over an extended period of time, with varying inlet and operating conditions.

Bibliography

[1] Teklehaimanot, G. Z., Kamika, I., Coetzee, M. A., and Momba, M. N., 2015, "Population Growth and Its Impact on the Design Capacity and Performance of the Wastewater Treatment Plants in Sedibeng and Soshanguve, South Africa," Environmental Management, **56**(4), pp. 984–997.

[2] S.L., P. P., G.C., D., and Ehrlich, 2008, "Human Appropriation of Renewable Fresh Water," American Association for the Advancement of Science, **271**(5250), pp. 785–788.

[3] Sonune, A. and Ghate, R., 2004, "Developments in wastewater treatment methods," Desalination, **167**(1-3), pp. 55–63.

[4] Metcalf and Eddy, 2002, *Wastewater Engineering: Treatment and Reuse*, McGraw - Hill, 4 ed.

[5] Wilson, T. E., 2005, *Clarifier Design*, 2.

[6] Rusten, B. and Odegaard, H., 2006, "Evaluation and testing of fine mesh sieve technologies for primary treatment of municipal wastewater," Water Science and Technology, **54**(10), pp. 31–38.

[7] Franchi, A. and Santoro, D., 2015, "Current status of the rotating belt filtration (RBF) technology for municipal wastewater treatment," Water Practice and Technology, **10**(2), pp. 319–327.

[8] Razafimanantsoa, V. A., Ydstebo, L., Bilstad, T., Sahu, A. K., and Rusten, B., 2014, "Effect of selective organic fractions on denitrification rates using Salsnes Filter as primary treatment," Water Science and Technology, **69**(9), pp. 1942–1948.

[9] Rusten, B., Secondary, C. A., Author, C., Rusten, B., Rathnaweera, S. S., Rismyhr, E., Sahu, A. K., Ntiako, J., and Rusten, B., 2017, "Rotating belt sieves for primary treatment , chemically enhanced primary treatment and secondary solids separation," Water Science and Technology.

[10] Loop, M., Higby, T., Martini, R., and Rusten, B., 2011, "Particle Size Separation Implications on COD Removal before BNR: A Case Study," Nutrient Recovery and Management, pp. 574–581.

[11] Jansen, R., 2016, "Successful pilot test of rotating belt filters," Filtration + Separation, **53**(4), pp. 26–27.

[12] Rusten, B., Razafimanantsoa, V. A., Andriamiarinjaka, M. A., Otis, C. L., Sahu, A. K., and Bilstad, T., 2016, "Impact of fine mesh sieve primary treatment on nitrogen removal in moving bed biofilm reactors," Water Science and Technology, **73**(2), pp. 337–344.

[13] Paulsrud, B., Rusten, B., and Aas, B., 2014, "Increasing the sludge energy potential of wastewater treatment plants by introducing fine mesh sieves for primary treatment," Water Science and Technology, **69**(3), pp. 560–565.

[14] Batstone, D. J. and Virdis, B., 2014, "The role of anaerobic digestion in the emerging energy economy," Current Opinion in Biotechnology, **27**, pp. 142–149.

[15] Tien, C., 2012, *Principles of Filtration*, Elsevier, Oxford, U.K.

[16] DeGroot, C. T., Sheikholeslamzadeh, E., Soleymani, A., Santoro, D., Batstone, D. J., and Rosso, D., 2015, "Understanding Primary Treatment Performance and Carbon Diver-

sion Potential of Rotating Belt Filters Using Computational Fluid Dynamics," WEFTEC, **2015**(6), pp. 1249–1262.

[17] DeGroot, C. T., Sheikholeslamzadeh, E., Santoro, D., Sarathy, S., Lyng, T.-O., Wen, Y., Daynouri-Pancio, F., and Rosso, D., 2016, "Dynamic Modeling of Rotating Belt Filters Enables Design Exploration and Advanced Sizing With Varying Influent Conditions," WEFTEC, **2016**(14), pp. 1158–1168.

[18] Bai, R. and Tien, C., 2005, "Further work on cake filtration analysis," Chemical Engineering Science, **60**(2), pp. 301–313.

[19] Tien, C. and Ramarao, B. V., 2011, "Revisiting the laws of filtration: An assessment of their use in identifying particle retention mechanisms in filtration," Journal of Membrane Science, **383**(1-2), pp. 17–25.

[20] Tien, C., 2002, "Cake filtration research—a personal view," Powder Technology, **127**(1), pp. 1–8.

[21] Teoh, S.-K., Tan, R. B. H., and Tien, C., 2006, "Analysis of Cake Filtration Data-A Critical Assessment of Conventional Filtration Theory," Wiley InterScience, **52**(10), pp. 3427–3442.

[22] Tien, C. and Ramarao, B. V., 2008, "On the analysis of dead-end filtration of microbial suspensions," Journal of Membrane Science, **319**(1-2), pp. 10–13.

[23] Tien, C. and Bai, R., 2003, "An assessment of the conventional cake filtration theory," Chemical Engineering Science, **58**(7), pp. 1323–1336.

[24] Tien, C., Ramarao, B. V., and Yasarla, R., 2014, "A blocking model of membrane filtration," Chemical Engineering Science, **111**, pp. 421–431.

[25] Osterroth, S., Preston, C., Markicevic, B., Iliev, O., and Hurwitz, M., 2016, "The permeability prediction of beds of poly-disperse spheres with applicability to the cake filtration," Separation and Purification Technology, **165**, pp. 114–122.

[26] Ho, C. C. and Zydney, A. L., 2000, "A Combined Pore Blockage and Cake Filtration Model for Protein Fouling during Microfiltration," J Colloid Interface Sci, **232**(2), pp. 389–399.

[27] Vafai, K. and Tien, C., 1981, "Boundary and inertia effects on flow and heat transfer in porous media," International Journal of Heat and Mass Transfer, **24**(2), pp. 195–203.

[28] Rusten, B. and Lundar, A., 2006, "HOW A SIMPLE BENCH-SCALE TEST GREATLY IMPROVED THE PRIMARY TREATMENT PERFORMANCE OF FINE MESH SIEVES," WEFTEC, pp. 1919–1935.

[29] Nield, D. A. and Bejan, A., 2013, "Mechanics of Fluid Flow Through a Porous Medium," Convection in Porous Media, pp. 1–778.

[30] Skjetne, E. and Auriault, J.-L., 2014, "High-Velocity Laminar and Turbulent Flow in Porous Media," CEUR Workshop Proceedings, **1225**(August 1999), pp. 41–42.

[31] Franklin, G. F., Powell, J. D., and Emami-Naeini, A., 2015, *Feedback Control of Dynamic Systems*, Pearson, 7 ed.

Chapter 4

Summary

4.1 Summary of Present Work

In the present work, a three dimensional idealized mesh filter model and one dimensional RBF model were developed to characterize the resistance across various mesh filters and the flow rate capacity and removal efficiency for a generic RBF, respectively. Each model was validated using experimental data gathered from experiments done to characterize mesh filters or pilot installations for the RBF model.

The mesh filter model was developed to accurately calculate the resistance across the mesh filter within an RBF unit, for various fluid velocities. To generalize the model and reduce computational time, the filter was modelled as a single, spatially period pore. Assuming a square pore geometry, the open area precentage was used to calculated the width and height of the domain and the thread diameter was assumed constant. Boundary conditions were developed by modeling the inlet pipe used in the experimental apparatus to correctly account for the fluid velocity and turbulence intensity profiles the mesh filter would experience. A sensitivity analysis showed that the turbulence intensity had little effect on the resulting flow resistance, allowing it to be held constant at 5%. However, the fluid velocity had a large effect. Using the peak velocity experienced by the filter in the experiment as the inlet velocity boundary condition in the CFD model, the best match between experimental and theoretical was found. The results from

this model were implemented into the one dimensional RBF model, allowing for the isolation of the cake resistance in Darcy's law.

A one dimensional model, based off of the model proposed by Sherratt et al. [1], was developed to predict the flow rate capcity and removal efficiency of a generic RBF unit. The cake layer and its effect on both flow rate capcity and removal efficiency was characterized by modeling two experiments: (i) gravity drainage column test, and (ii) sieve test. The column test was modelled using a double exponential formulation which characterized the change in water height in the column over time. The double exponential allows for the instantaneous fluid velocity to be determined and by applying that to the formulation generated from the mesh filter CFD model, the mesh resistance versus time was characterized. This allows for the isolation of the cake resistance term in Darcy's law, thereby allowing the cake resistance versus filtered volume to be deteremined. The sieve test was modelled using a single exponential formulation to characterize the effluent TSS concentration for a given filtered volume, with a known TSS concentration. In the RBF code, the cumulative filtered volume is tracked for each filtration cycle, therefore, using the sieve test model allows for the effluent TSS concentration to be determined thereby allowing the removal efficiency to calculated. The combination of the column test and sieve test models allows for flow rate capcity and removal effficiency curves to be determine for a given RBF unit across a range of belt speeds. To increase the applicability, the RBF model was then extended to include TSS scaling, a PID controller and parameter optimization. TSS scaling allowed the RBF model to predict pilot performance over a extended period of time with varying inlet TSS conditions (which is seen in pilot installations). The PID controller allowed for the characterization of the dynamic response of an RBF unit to varying inlet conditions. It was also be used as a tool to optimize the gain values for an RBF pilot for various water qualities and operational goals. Finally, the parameter optimization was included to account for cake errosion during the filtration cycle and/or imperfect cleaning of the mesh filter, both of which effect predicted flow rates considerably. By optimizing the parameters obtained from a column test to pilot data, close agreement was found between predicted and

observed pilot flow rates.

4.2 Suggestions for Future Work

4.2.1 Parametric Study for Mesh Filter CFD Model

In the present work, the mesh filter model was only developed to characterize two mesh filters. To make the model more generalized, it is recommended that a parametric study be done on the effect of varying the thread diameter and open area percentage on the resulting pressure drop. This would allow the results to be truly non-dimensionalized and the model would be more applicable to other filters.

4.2.2 Inclusion of CEPT

Chemically enhanced primary treatment (CEPT) is a commonly used method of increasing the removal efficiency in the primary treatment stage. A chemical coagulant, either ferric chloride or cationic polymer (for its ability to increase the strength of the amalgamated particulate, also known as flocs), is introduced into the influent wastewater stream to form flocs, which are easier to remove given their larger size. In the present study, CEPT was not considered. Given that CEPT is being included in RBF pilots, its important to include this feature in the model to observe its effect on flow rate capacity and removal efficiency. The method for doing this would be to consider the cake resistance term, R_{cake}, in Darcy's law as a series of various cake resistances depending on the influent solids particle size distribution. Experimental work can be done to determine the contribution to the cake resistance each particle size makes. This allows an understanding of how large particles, created during CEPT, effects the overall cake resistance.

4.2.3 PID Replication of Pilot Data

Presently, the PID controller in the RBF model has only been used with hypothetical data. To truly predict how an RBF unit behaves under various circumstances, it is recommended that the PID controlled model be extend to accept influent TSS concentrations and flow rates recorded from an RBF pilot installation. The results can be used to predict dynamic RBF performance and also be used as a method of optimizing the gain values used in RBF pilots.

4.2.4 Wastewater Treatment Plant Modeling

In the present work, only the performance of a single RBF has been modelled. It is suggested that the models developed (mesh filter CFD model and RBF model) be used to determine the number of RBF units and the appropiate mesh size needed to meet WWTP flow rate and removal efficiency objectives.

Bibliography

[1] Sherratt, A., Degroot, C. T., Santoro, D., Daynouri, F., Mao, S., and Straatman, A. G., 2017, "Development of a Volume-Based Filtration Model for Predicting Full-Scale Rotating Belt Filter Performance in Wastewater Applications," WEFTEC.

Chapter 5

Appendix 1

Case 1

Table 5.1: Case 1 column test parameters.

h_0 [m]	A [m]	α [1/s]	β [1/s]
0.738	0.337	0.013	2.176

Case 2

Table 5.2: Case 2 sieve test parameters.

C_0 [mg/L]	γ [m^2/m^3]
180.23	0.187

Case 3

Table 5.3: Case 3 column and sieve test parameters values and TSS concentration.

h_0 [m]	A [m]	α [1/s]	β [1/s]	C_0 [mg/L]	γ [m^2/m^3]
1	0.6	1	0.1	220	0.35

Case 4

Table 5.4: Case 4 column test parameters.

h_0 [m]	A [m]	α [1/s]	β [1/s]
0.936	0.227	3.03	0.002

Case 5

Table 5.5: Case 5 column test parameters and influent TSS value.

h_0 [m]	A [m]	α [1/s]	β [1/s]	TSS [mg/L]
0.795	0.523	0.008	1.424	353

Case 6

Table 5.6: Case 6 column test parameters and influent TSS value.

h_0 [m]	A [m]	α [1/s]	β [1/s]	TSS [mg/L]
0.669	0.410	0.005	2.251	693

Case 7

Table 5.7: Case 7 optimized column test parameters.

h_0 [m]	A [m]	α [1/s]	β [1/s]
0.795	0.387	0.008	1.424

Curriculum Vitae

Name:	Anthony Sherratt
Post-Secondary Education and Degrees:	The University of Western Ontario London, Ontario, Canada 2012 - 2016 B.E.Sc. University of Western Ontario London,Ontario, Canada 2016 - 2018 M.E.Sc.
Honours and Awards:	Deans Honour List 2015-2016
Related Work Experience:	Teaching Assistant *MME 2204 - Thermodynamics I* *MME 3334 - Thermodynamics II* *MME 2213 - Engineering Dynamics* *MME 3381 - Kinematics and Dynamics of Machines* *MME 4423 - Internal Combustion Engines* The University of Western Ontario 2016 - 2018

Publications:

Sherratt, A., DeGroot, C.T., Santoro, D., Daynouri-Pancino, F., Mao, S., Straatman, A.G., 2017,"Development of a Volume-Based Filtration Model for Predicting Full-Scale Rotating Belt Filter Performance in Wastewater Applications",WEFTEC 2017, Chicago, USA.

Sherratt, A., DeGroot, C.T., Straatman, A.G., Santoro, D., 2018, "A Numerical Approach for Determining the Resistance of Fine Mesh Filters", Submitted to C.S.M.E.

Sherratt, A., DeGroot, C.T., Straatman, A.G., Santoro, D., 2018, “A Mathematical Model of a Rotating Belt Filter”, Under review by Trojan Technologies.